PERMITTIVITY MEASUREMENTS IN TIME DOMAIN

A Thesis

Presented to

The Faculty of Graduate Studies and Research

University of Manitoba

In Partial Fulfillment

of the Requirements for the Degree

Master of Science

Agricultural Engineering Department

by

MAGDY FAHMY ISKANDER

October, 1972

ABSTRACT

A novel time domain (transient) method for (broad band) measurement of the dielectric properties of materials is described. Special emphasis is placed on testing the biological substances, where essentially a very small sample size is required. Theoretical analysis of the time dependence of the reflection coefficient, following application of a step voltage to a shunt capacitor located at the end of a transmission line and filled with the dielectric under test, is given. Analysis and calculations of the overall uncertainty of permittivity measurements as well as a technique to choose the optimum value of the capacitance for a specified frequency band are presented. The effect of fringing fields is studied and a correction factor is provided. Feasibility of the proposed method was evaluated by making some measurements. Experimental results are presented and limitations of the method discussed.

ACKNOWLEDGEMENTS

The author wishes to acknowledge his sincere thanks to all those who assisted and encouraged him during the course of this work.

In particular, he is pleased to acknowledge his indebtedness to Dr. S.S. Stuchly for his continuous interest, helpful advice, cheerful and able guidance in all phases of this work.

Special thanks to Dr. M.A.K. Hamid and Dr. J.S. Townsend for their interest and valuable comments.

Acknowledgement is extended to Mr. Jack Putnam for his skilled and precise machining of the test capacitor.

This research was supported by the Manitoba Department of Agriculture, the National Research Council of Canada and the Faculty of Graduate Studies of the University of Manitoba.

TABLE OF CONTENTS

LIST OF FIGURES

Page

Page

LIST OF TABLES

CHAPTER 1

INTRODUCTION

Investigation of the dielectric properties of biological substances and their frequency and temperature dependence provides very valuable information about their nature. From these properties one can determine the state of water (free or bound), molecular structure and the hydration process which are of primary importance in biochemistry and biophysics [1, 5].

A macroscopic description of the dielectric properties of a material is provided by the complex dielectric permittivity $\varepsilon^* = \varepsilon' - j\varepsilon''$. The significant variables on which ε^* depends, in decreasing order of importance, are the frequency, the temperature, the pressure, and the intensity of the applied electric field. Methods of measuring the real and imaginary parts of ε^* as a function of these variables are described comprehensively in the literature [2 - 4].

The choice of a method depends principally on the frequency and very little on the temperature. Although ε^* is usually defined in terms of an experiment using sinusoidal electric fields (frequency domain measurements), experiments using other time-dependent fields may also be used.

If $\varepsilon'' \neq 0$ in the range 10^{-3} to 10^{3} Hz, ε^* may be determined by transient methods. A step or ramp voltage is applied to a condenser and the time dependence of the electric displacement D may be used to compute ε^* of an enclosed sample. An experiment using sinusoidal fields is possible at these frequencies (and higher) as well. For frequencies from 10^{-3} Hz to 10 MHz the condenser with a sample may be treated as a two- or three-terminal impedance (two-terminal impedance if one terminal is connected to a shield; three terminal impedance if neither terminal is connected to a shield). The impedance is measured by a bridge which varies in design depending on the frequency range. At very low frequencies a long time is required to complete a cycle and reach the steady state, so bridges which permit relatively rapid measurements are desirable.

At frequencies of a few MHz the condition, required for use of conventional circuit theory, that the dimensions of the sample be small compared with the wavelength is no longer valid. Circuit theory concepts, however, may be used to about 200 MHz by employing resonant circuits. The dielectric permittivity is computed from the capacitance change required to restore the circuit to resonance after introducing the sample. When the sample extends over an appreciable part of a wavelength it becomes necessary to confine the electric and magnetic fields inside conductors. The permittivity may be determined from the interaction of waves travelling on a transmission line with a sample placed in the line. A resonant system bound by conductors, which is analogous to a resonant circuit, may be constructed.

The upper frequency limit of the transmission-line apparatus is limited by the difficulty of fabricating components of precise geometry. The upper limit is perhaps 75 GHz. Electromagnetic waves may interact with the sample in free space. The basic equations are similar in many ways to those for transmission-line measurements. Free-space methods are unsuitable below 40 GHz since the optical methods require that the sample be large compared with a wavelength so the effects of diffraction may be neglected.

In the first section of this chapter the current state-of-art in the permittivity measurement of biological substances, a review of some important applications, and a summary of some important aspects to be considered with regard to instrumentation used are discussed. In the second section a general description of the proposed problem and the purpose of the investigations are presented.

1.1.1 Dielectric properties of biological substances

The electric properties of biological materials have been studied ever since suitable electrical techniques became available for this purpose. Earlier contributions, restricting the discussion to the "passive" electric properties, did not help much toward understanding the factors responsible for the electrical properties of tissues. After 1940 techniques became available for investigation of the electrical properties at ultra high and low frequencies. The frequency range so far explored extends from 5 Hz up to 30 GHz [5].

Figure 1 shows, as a typical example for biological materials, the frequency-dependence of the dielectric constant of muscular tissue. It demonstrates three dispersions (α,β,γ), each characterizing a separate relaxation mechanism. A study of the linear electric properties of biological systems is identical with an analysis of the mechanisms responsible for the three anomalous dispersions. This behaviour applies to the various types of biological materials as given in Table 1 [5]. It is apparent from Table 1 that the α- and β-dispersions are not due to the water and electrolyte content of the biological samples. The total change of the dielectric constant ($\Delta\varepsilon$) as the frequency varies throughout the dispersion range of interest is termed dispersion magnitude. Its value depends on the particular material involved, its concentration, and other factors such as type of ionic environment, temperature, etc. However, the following statement may be made: the dielectric constants observed

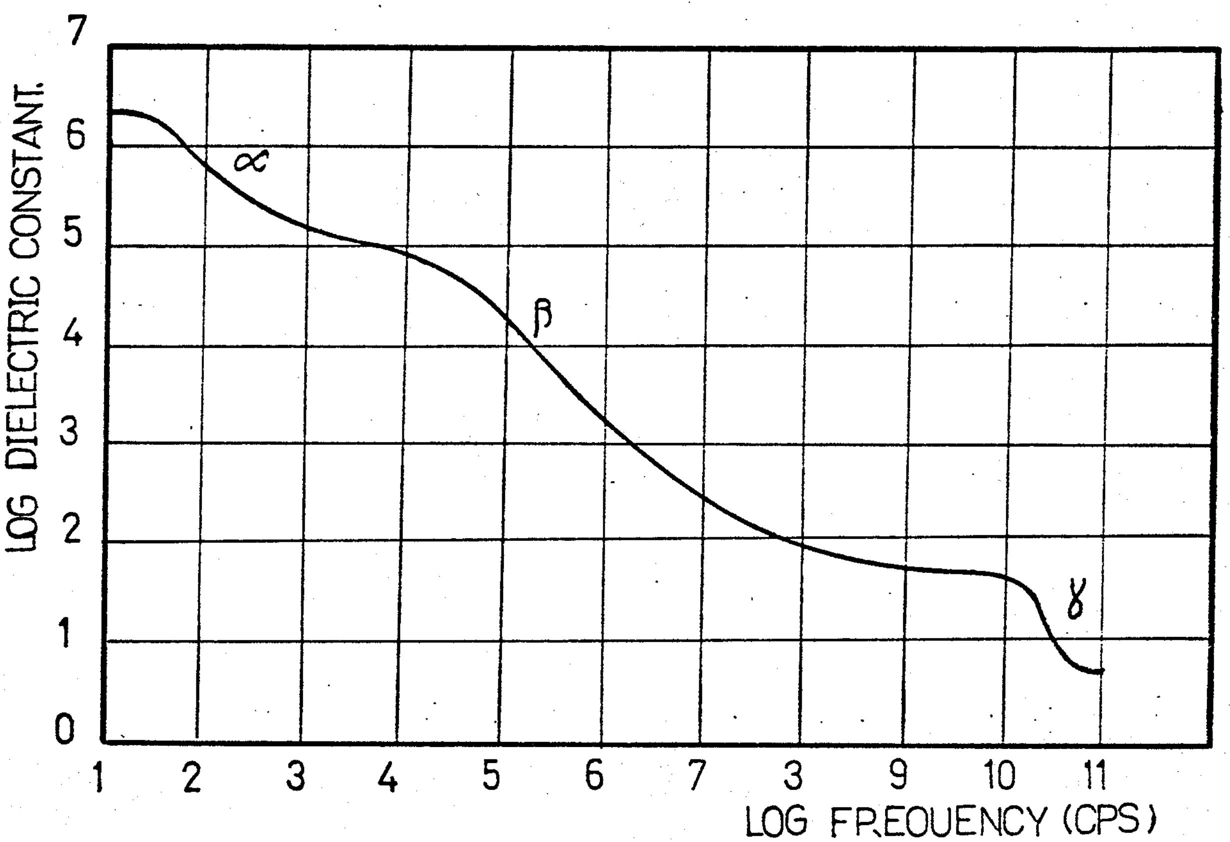

Fig.1 Frequency dependence of the dielectric constant of muscular tissue. The dependence is characterized by three dispersions(α, β, γ), each due to a different mechanism.

Table 1

Characteristic Frequencies of Major Dispersions

	α-Dispersion	β-Dispersion	γ-Dispersion
Water and Salt Solutions	none	none	20,000 Mc
Protein and Other Macro-Molecular Suspensions	none	1-10 Mc	20,000 Mc
Subcellular Particles (Cell Nuclei)	?	1-10 Mc	20,000 Mc
Cell Suspension, Bacteria and Tissues	0.1-10 Kc	0.1-10 Mc	30,000 Mc

are often extremely high compared with those of homogeneous liquids and solids due to the heterogeneous structure of biological cell suspensions and tissues and ion transfer processes [6].

A survey of published tissue data is presented in Table 2 [6]. It is clear from Table 2 that dielectric constants range from a few units to more than a million.

1.1.2 Applications of dielectric properties measurement of biological substances

The study of the dielectric properties of biological substances has become increasingly important due to their numerous potential applications in biophysics and biochemistry. The following summarizes different applications of high frequency measurements [7]:

(a) Investigation of the health hazard associated with the exposure of human beings to powerful sources of electromagnetic radiation, e.g., radar equipment. There have been reports about ill effects, which may multiply as more and more powerful equipment is developed. Careful analysis is required [8].

(b) Electromagnetic radiation has been used in clinics for the purpose of deep tissue heating. Further development in this field depends on additional biophysical research carried out in cooperation with microwave engineers.

(c) Electromagnetic heating for material processing.

Table 2

Electrical Properties of Body Tissues

		A	B	C	D	E	F	G	H	I
	Frequency	Muscle	Liver	Lung	Spleen	Kidney	Brain	Fatty Tissue	Bone and Bone Marrow	White Blood
1	100 cps	800×10^3	900×10^3	450×10^3				150×10^3		
2	100 cps	1000×10^3								
3										
4		130×10^3	150×10^3	90×10^3				50×10^3		
5	1 kc	170×10^3								2000
6		100×10^3								
7		50×10^3	50×10^3	30×10^3				20×10^3		
8	10 kc	90×10^3								2810
9		50×10^3								
10										
11	100 kc	30×10^3								2740
12		20×10^3	$(7-12) \times 10^3$							
13										
14	1 Mc									2010
15		2×10^3	$(1.2-2) \times 10^3$							
16										
17	10 Mc									200
18										
19			65-75					8-13		
20	100 Mc									
21		69-73	72-74		88-90	83-84	70-75			72-74
22		49-52	46-47					4.3-7.8	4.3-7.8	58-62
23	1000 Mc	53-55	44-52	35		53-56		3.2-6		63
24		61	50					9.5		
25		40-42	34-38					3.5-3.9	4.4-6.6	50-52
26	10,000 Mc	29						3.6	6	45

Here again, ultimate performance can be expected only if knowledge of the electrical properties of various types of plant and animal tissues have been established.

(d) Attempts to derive from UHF measurements a quantity which is of great interest to biochemists, namely the amount of bound water associated with protein molecules [9].

1.1.3 Instrumentation requirements

The following summarizes the most important aspects to be considered with regard to the instrumentation used for the above-mentioned investigations [7]. It is desirable to

(a) measure over a wide and continuous frequency spectrum in order to recognize the frequency dependence involved.

(b) operate with small samples. Often it is difficult to obtain more than a few cc of biological material.

(c) vary temperature in order to recognize the temperature dependence of dielectric parameters.

(d) keep the sample under observation in order to avoid errors which may arise from the presence of gas bubbles or from settlement of the cells in suspension, etc.

(e) define the geometric size of the sample in a precise and yet simple manner. Since the biological material is not available in solid form, sample boundaries must be established which confine the sample in a well-defined manner. These sample walls can not be permitted to affect the measurements in an unpredictable manner.

1.2 Description of the problem and purpose of the investigation

Currently used methods both in frequency and time domains, although highly refined and accurate [10 - 13], do not meet all the requirements imposed by experiments with biological substances. In particular, a relatively large sample is required to fill a test capacitor or a section of a coaxial line, especially when substances with long relaxation times are measured [12] and [13].

In this thesis a novel technique for permittivity measurements in time domain, which utilizes a small shunt capacitor terminating a coaxial line section as a sample holder is described. Analysis of the time dependence of the reflection coefficient following application of a step voltage to a shunt capacitor located at the end of a transmission line and filled with the dielectric material under test is given. Analysis and calculation of the overall uncertainty of permittivity measurements as well as experimental results are presented. Limitations of the method as well as suggestions for future work are given.

CHAPTER 2

TIME DOMAIN METROLOGY

It is only recently that measurement of the transient response of microwave systems directly in time domain has become practicable. This has led to growing interest in the concept of specifying broad-band performance solely by a transient-response measurement. Due to the wide instantaneous spectrum of the pulse, frequency information can be obtained over several decades by a single measurement of the subnanosecond rise-time response of the system under test by applying Fourier transforms. This method is especially suited for characterizing broad band components with limited transient response.

Nicolson [14] presented some results of the use of time-domain techniques to obtain such data as the S-parameters of networks, the constitutive parameters of microwave materials, the driving point impedance and transfer function of microwave antennae, and the frequency domain scattering parameters of conducting surfaces in free space in the range of 0.1 to 10 GHz. There is no doubt that there will be a rapid increase in new applications due to the advantages offered by the time domain technique.

2.1 Time and frequency domain techniques for permittivity measurements

Generally the measurement of the dielectric behaviour of solids and liquids are made by placing the substance between the two plates of a capacitor (at low frequency) or in a coaxial line and measuring the complex impedance at different frequencies. A number of measurements over a wide frequency range is required for complete characterization which is time consuming and demands a considerable investment in instrumentation particularly for the microwave region. Therefore, in spite of its usefulness, this method has found rather limited applications.

One can obtain the same information over a wide frequency range in only a fraction of a second by making the measurement not in the frequency domain but in the time domain, using a pulse that simultaneously contains all the frequencies of interest. This pulse method has been used for low frequency investigations on dielectrics. Modern tunnel diode pulse generators and wide band sampling oscilloscopes extend this method into the microwave region where saving in time and equipment are most pronounced.

Briefly speaking, time-to-frequency domain techniques do offer the following advantages over more conventional techniques:

(a) Simplicity of instrumentation.

The three basic elements of the measurement system are a subnanosecond rise-time pulse generator, a broad band sampling oscilloscope and an instrumentation computer.

(b) Time windowing.

The unique ability to carry out frequency analysis of only certain regions of the time domain waveform allows the elimination of unwanted reflections.

(c) Simultaneous display of time and frequency domain responses.

Frequently, useful information about the operation of a microwave network can be obtained from the juxtaposition of these two responses.

2.2 Survey of the literature

Sometimes in the past, the transient method has been applied for low frequency investigation of dielectrics. The application of this technique in high frequency applications had to await the development of subnanosecond rise-time pulse generators and broad-band sampling oscilloscopes.

H. Fellner-Feldegg [12] measured the high frequency and low frequency dielectric constant κ_∞ and κ_o in time domain by measuring the reflection of a voltage step from the air-dielectric interface (Fig. 2(a)). The shape of the reflected signal gives information about the high frequency

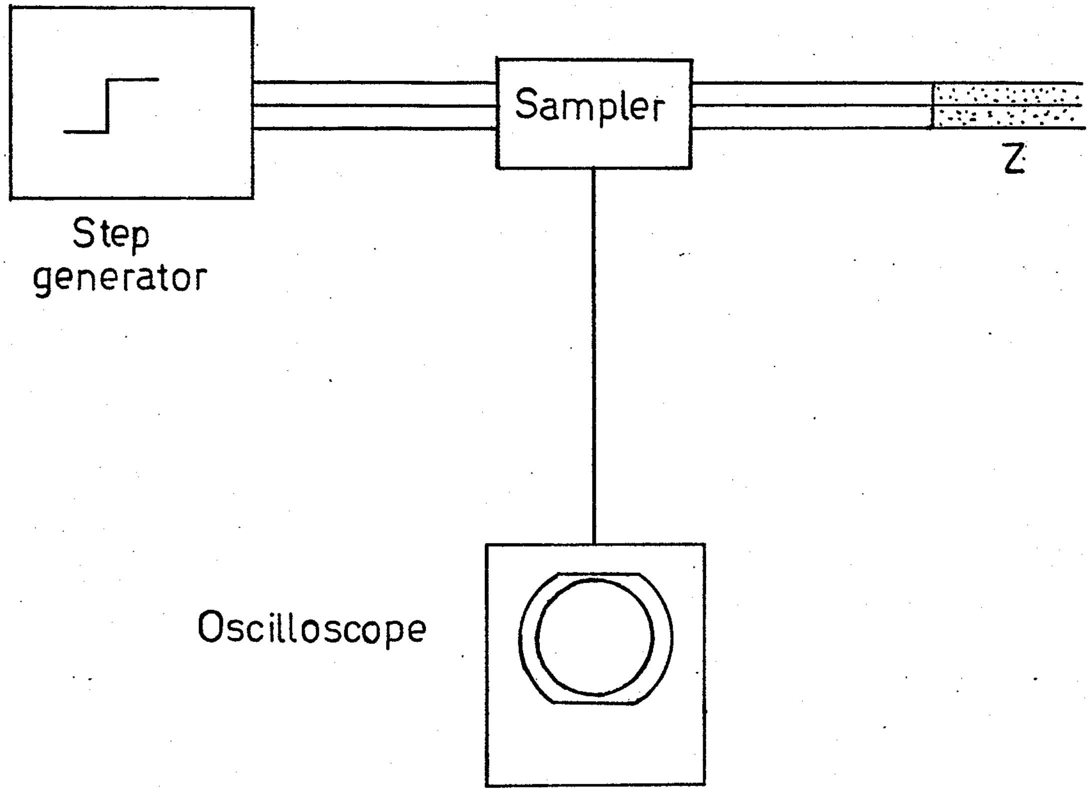

Fig.2a Time domain reflectometer setup

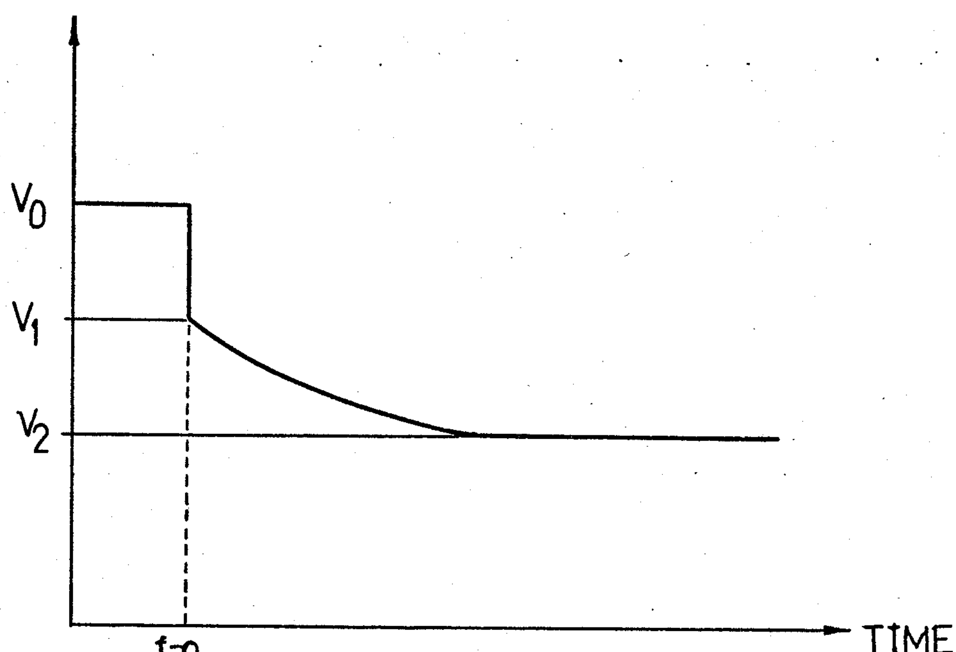

Fig.2.b Typical reflection of a step pulse V_0 from an air-dielectric interface.

and low frequency dielectric constants κ_∞, κ_o, respectively, as shown in Fig. 2(b). Here

$$\kappa_\infty = \left(\frac{1-\rho_\infty}{1+\rho_\infty}\right)^2 \quad , \quad \kappa_o = \left(\frac{1-\rho_o}{1+\rho_o}\right)^2$$

where

$$\rho_\infty = \frac{v_1 - v_o}{v_o} \quad , \quad \rho_o = \frac{v_2 - v_o}{v_o}$$

are the reflection coefficients, v_o is the amplitude of the incident step pulse, $v_1 - v_o$ the amplitude of the reflected pulse at the time $t = 0$, and $v_2 - v_o$ the reflected pulse height when the relaxation of the dielectric is complete. For the determination of the relaxation time [13], he used the Laplace transform to derive an expression for the reflected voltage as a function of time, for the Debye dielectrics, in an infinite series form. This series, after being computed and plotted, for different values of κ_o and κ_∞ of practical interests, facilitates the determination of the relaxation time.

A.M. Nicolson and G.F. Ross [10] used another time domain technique for the determination of the complex permeability and permittivity of linear materials in the frequency domain. The technique described involves placing an unknown sample in a microwave TEM-mode fixture and exciting the sample with a subnanosecond base band pulse (Fig. 3(a)). The fixture is used to facilitate the measurement of the forward and back-scattered voltage components, $S_{21}(t)$ and $S_{11}(t)$, respectively. Because the forward and

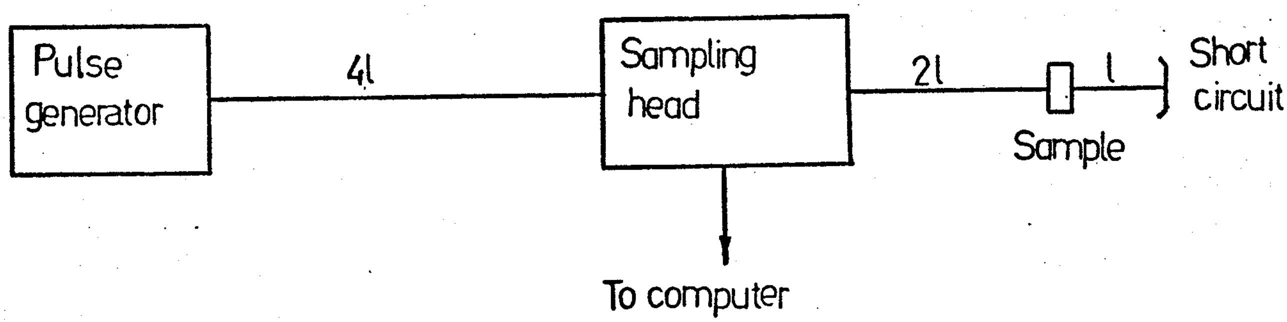

Fig3.a Time-domain measurement system

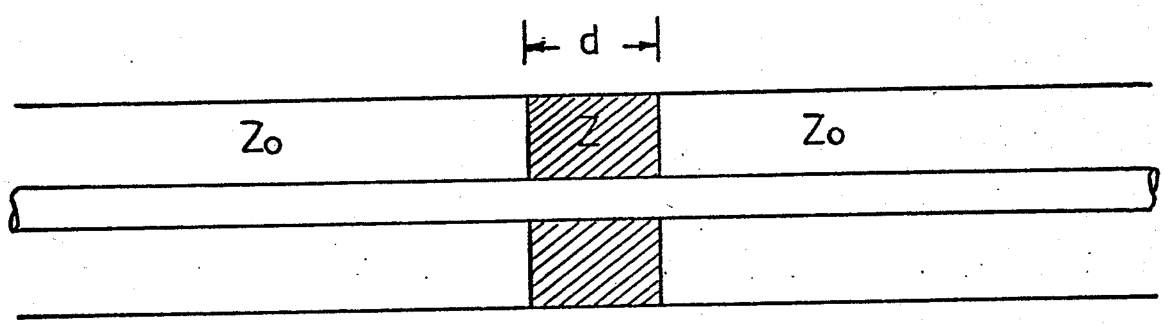

Fig.3.b A coaxial line with annular disk of material to be measured inserted

back-scattered time domain "signatures" are uniquely related to the intrinsic properties of the materials under test, namely ε^* and μ^*, it is possible to determine the real and imaginary parts of ε^* and μ^* as functions of frequency through the application of the discrete Fourier transform (DFT) to the measured quantities in time domain. The samples used were in annular disc form installed in a coaxial air-filled line with characteristic impedance Z_o, as shown in Fig. 3(b). The substances used have very short relaxation times (e.g., nylon and plexiglas) and so the required sample thickness is relatively small (0.05" - 0.1"). It is clear that this technique will necessitate a relatively larger sample thickness for the measurements of dielectrics with long relaxation times.

In conclusion, the currently used methods, both in frequency and time domains, although highly refined and accurate do not meet all the requirements imposed by experiments with biological substances; specifically, a relatively large sample is required for substances with long relaxation times.

In the proposed technique a small shunt capacitor terminating a coaxial line section is used as a sample holder. This technique gives all necessary information on the frequency behaviour of the tested substance, while the required sample volume is of the order of a few cubic millimeters. The greatest assets of the proposed method are its speed, simplicity, relative ease of data evaluation and the small sample required.

CHAPTER 3

THEORY

When a time domain reflectometer (TDR) is used, a very fast rise (subnanosecond) voltage step is generated, while both incident and reflected waves are picked up by a high impedance sampler and displayed on the screen of a broad band sampling oscilloscope. The deflection of the oscilloscope trace is proportional to the algebraic sum of the incident and reflected waves. Assuming the amplitude of the incident wave equal to unity, the sum of the incident and reflected waves is equal to $f(t)$ and $f(t) = 1$ for $t < 0$ and $f(t) \neq 1$ for $t > 0$. From transmission line theory, the reflection coefficient for a transmission line terminated by a load impedance $Z_L(p) = \frac{1}{pC(p)}$ is

$$\rho(p) = \frac{1 - Z_o pC(p)}{1 + Z_o pC(p)} \tag{1}$$

where $p=j\omega$ and ω is the angular frequency, and $C(p)$ is the capacitance of the capacitor terminating the transmission line. The capacitor, as shown in Fig. 4(a), consists of a coaxial cavity closed at one end with a conducting cover plate and the tip of the inner conductor at the other end.

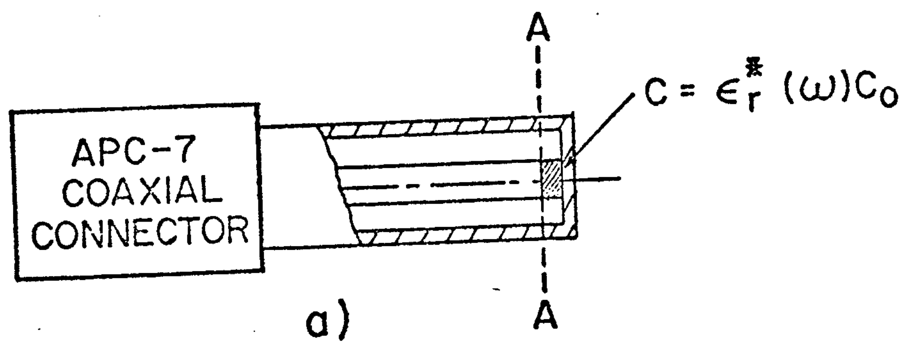

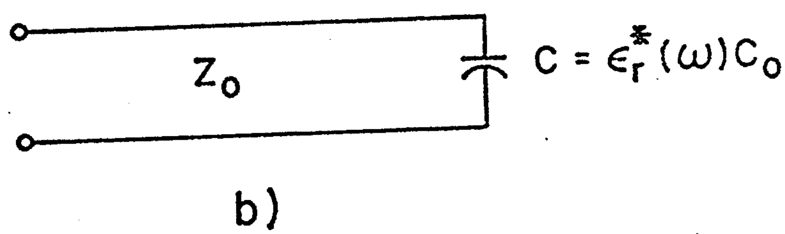

Fig.4. The sample holder a) APC-7 coaxial sample holder and b) its equivalent circuit.

A gap between the two conducting planes can be varied depending on the required capacitance. In reference to the plane A-A, the inner conductor is shown to be terminated to ground through a capacitance C, Fig. 4(b). When the capacitor is filled with the test dielectric $C(p) = C_o\varepsilon_r^*(p)$†, where C_o is the capacitance of the air filled capacitor, then the reflection coefficient is

$$\rho(p) = \frac{1 - pC_oZ_o\varepsilon_r^*(p)}{1 + pC_oZ_o\varepsilon_r^*(p)} \tag{2}$$

From Eqn. (2) the frequency dependence of the reflection coefficient can be obtained by substituting the specific function $\varepsilon_r^*(p)$ representing a particular mechanism of dispersion. We shall consider some specific mechanisms, which are of potential interest in biological studies, namely:

Ohmic dispersion:

$$\varepsilon(p) = \varepsilon_\infty + \frac{\kappa}{p}\ ,\ \kappa = \frac{\sigma}{\varepsilon^o}$$

Resonance dispersion:

$$\varepsilon(p) = \varepsilon_\infty + \tfrac{1}{2}(\varepsilon_o - \varepsilon_\infty)\left(\frac{1 - \tau p_o}{1 + \tau(p - p_o)} + \frac{1 + \tau p_o}{1 + \tau(p + p_o)}\right)$$

---

† This assumption is not absolutely correct because of fringing field effects, but is justified to 0.5 percent accuracy in Chapter 4.

Debye dispersion:

$$\varepsilon(p) = \varepsilon_\infty + \frac{\varepsilon_o - \varepsilon_\infty}{1 + \tau p}$$

The case of Debye dispersion with distributed relaxation times will be studied also.

For each of these dispersion mechanisms, the system response displayed on the sampling oscilloscope screen is theoretically derived so it may be used for checking the experimental data and necessary corrections can be easily provided (e.g. corrections for finite rise time of the system).

3.1.1 · Dielectrics showing ohmic dispersion

The frequency dependence of the complex permittivity for dielectrics which can be best described as showing ohmic dispersion at the frequency band of interest, is given by

$$\varepsilon(p) = \varepsilon_\infty + \frac{\kappa}{p} \quad , \quad \kappa = \frac{\sigma}{\varepsilon^o} \qquad (3)$$

where σ is the conductivity of the material, ε^o the absolute dielectric constant of free space. Substituting Eqn. (3) into Eqn. (2)

$$\rho(p) = \frac{1 - Z_o C_o p(\varepsilon_\infty + \frac{\kappa}{p})}{1 + Z_o C_o p(\varepsilon_\infty + \frac{\kappa}{p})}$$

$$\rho(p) = -1 + \frac{2}{1 + Z_o C_o \varepsilon_\infty p + \kappa Z_o C_o}$$

System response to a step function excitation is

$$\Gamma(p) = \frac{\rho(p)}{p}$$

hence

$$\Gamma(p) = -\frac{1}{p} + \frac{2\ Z_o C_o \varepsilon_\infty}{p\left(\left(\frac{1 + \kappa Z_o C_o}{Z_o C_o \varepsilon_\infty}\right) + p\right)} \qquad (4)$$

System response on the oscilloscope screen which is a sum of the incident and reflected waves can be obtained by the inverse Laplace transform of the elements of Eqn. (4)

$$f(t) = \frac{2}{1 + \kappa Z_o C_o} \left(1 - \exp -\left(\frac{1 + \kappa Z_o C_o}{Z_o C_o \varepsilon_\infty}\right) t\right) \qquad (5)$$

The behaviour of the system described by Eqn. (5) is presented by a simple equivalent circuit shown in Fig. 5, where

$$Y = pC = pC_o \varepsilon_r = pC_o(\varepsilon_\infty + \frac{\kappa}{p}) = pC_o \varepsilon_\infty + C_o \kappa$$

3.1.2 Dielectrics showing resonance dispersion

This dispersion mechanism can be described by the

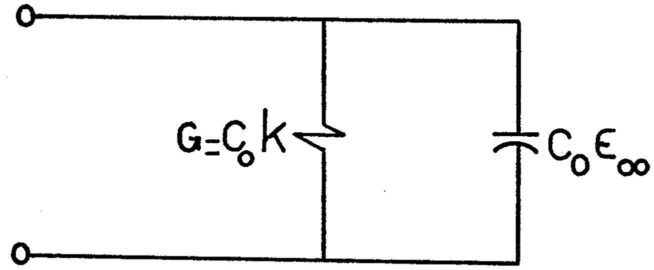

Fig.5. Equivalent circuit for the sample holder filled with a dielectric showing the Ohmic dispersion

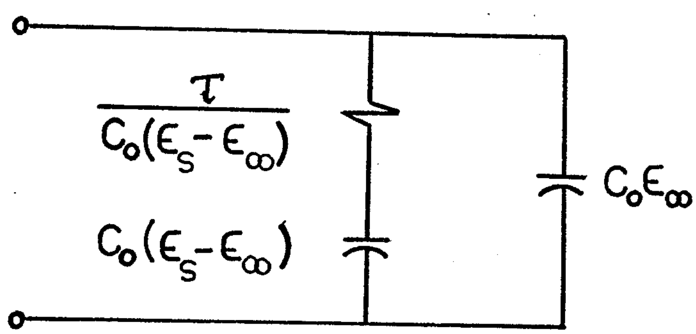

Fig.6. Equivalent circuit for the sample holder filled with a dielectric showing the Debye dispersion

expression [15]

$$\varepsilon(p) = \varepsilon_\infty + \tfrac{1}{2}(\varepsilon_o - \varepsilon_\infty)\left(\frac{1-\tau p_o}{1+\tau(p-p_o)} + \frac{1+\tau p_o}{1+\tau(p+p_o)}\right) \qquad (6)$$

where $p_o = j\omega_o = j2\pi f_o$ and f_o is the resonance frequency. Substituting Eqn. (6) into Eqn. (2)

$$\rho(p) = \frac{1 - pZ_oC_o\{\varepsilon_\infty + \frac{1}{2}(\varepsilon_o-\varepsilon_\infty)(\frac{1-\tau p_o}{1+\tau(p-p_o)} + \frac{1+\tau p_o}{1+\tau(p+p_o)}\}}{1 + pZ_oC_o\{\varepsilon_\infty + \frac{1}{2}(\varepsilon_o-\varepsilon_\infty)(\frac{1-\tau p_o}{1+\tau(p-p_o)} + \frac{1+\tau p_o}{1+\tau(p+p_o)}\}}$$

Let $1-\tau p_o = U_1$, $1+\tau p_o = U_2$, $\varepsilon_o - \varepsilon_\infty = \Delta$, and $\varepsilon_o + \varepsilon_\infty = \Delta'$, then

$$\rho(p) = \frac{1 - pZ_oC_o\{\varepsilon_\infty + \frac{\Delta}{2}(\frac{U_1}{U_1+\tau p} + \frac{U_2}{U_2+\tau p})\}}{1 + pZ_oC_o\{\varepsilon_\infty + \frac{\Delta}{2}(\frac{U_1}{U_1+\tau p} + \frac{U_2}{U_2+\tau p})\}} \qquad (7)$$

Eqn. (7) can be rearranged in the form

$$\rho(p) = -\frac{p^3 - F_2p^2 - F_1p - F}{p^3 + F_2'p^2 + F_1'p + F}$$

where

$$F = \frac{U_1U_2}{Z_oC_o\varepsilon_\infty\tau^2}$$

$$F_1 = \frac{(2\tau - Z_o C_o U_1 U_2 \varepsilon_o)}{\tau^2 Z_o C_o \varepsilon_\infty} \quad , \quad F_1' = \frac{(2\tau + Z_o C_o U_1 U_2 \varepsilon_o)}{\tau^2 Z_o C_o \varepsilon_\infty}$$

$$F_2 = \frac{\tau^2 - Z_o C_o \tau \Delta'}{\tau^2 Z_o C_o \varepsilon_\infty} \quad , \quad F_2' = \frac{\tau^2 + Z_o C_o \tau \Delta'}{\tau^2 Z_o C_o \varepsilon_\infty}$$

System response to a step function excitation is

$$\begin{aligned} \Gamma(p) &= \frac{\rho(p)}{p} \\ &= -\frac{1}{p}\,\frac{p^3 - F_2 p^2 - F_1 p - F}{p^3 + F_2' p^2 + F_1' p + F} \qquad (8) \\ &= -\frac{R(p)}{q(p)} \\ &= \frac{A}{p} + \frac{B}{p-S_1} + \frac{C}{p-S_2} + \frac{D}{p-S_3} \end{aligned}$$

Where S_1, S_2 and S_3 are the roots of the denominator of Eqn. (8). A, B, C, and D are defined in terms of these roots as follows:

$$A = \frac{F}{S_1 S_2 S_3} = 1$$

$$B = \frac{S_1^3 - F_2 S_1^2 - F_1 S_1 - F}{S_1(S_1 - S_2)(S_1 - S_3)}$$

$$C = \frac{S_2^3 - F_2 S_2^2 - F_1 S_2 - F}{S_2(S_2 - S_1)(S_2 - S_3)}$$

and

$$D = \frac{S_3^3 - F_2 S_3^2 - F_1 S_3 - F}{S_3(S_3-S_1)(S_3-S_2)}$$

Hence, the system response on the oscilloscope screen, which is a sum of the incident and reflected waves, can be obtained by the inverse Laplace transform and using the Heaviside expansion formula

$$f(t) = 1 + \Gamma(t) = 1 + \mathcal{L}^{-1}\{-\frac{R(p)}{q(p)}\}$$

$$= 1 + \sum_{r=1}^{n} \frac{R(\alpha_r)}{q'(\alpha_r)} e^{\alpha rt}$$

where q' is the derivative of q with respect to p and α_r are the roots 0, S_1, S_2 and S_3. Hence

$$f(t) = 2 + Be^{S_1 t} + Ce^{S_2 t} + De^{S_3 t}$$

3.1.3 Dielectrics showing the Debye dispersion

A polar dielectric of the Debye type has a complex dielectric constant which depends on frequency according to the equation

$$\varepsilon(p) = \varepsilon_\infty + \frac{(\varepsilon_o-\varepsilon_\infty)}{1+p\tau} \tag{9}$$

where ε_o and ε_∞ are the dielectric constants at frequencies very low and very high with respect to the relaxation frequency, respectively, and τ is the relaxation time. Substituting Eqn. (9) into Eqn. (2) and putting $A = \tau - C_o Z_o \varepsilon_o$; $B = \frac{1}{C_o Z_o \varepsilon_\infty \tau}$; and $C = \tau + C_o Z_o \varepsilon_o$, Eqn. (2) can be written in the form

$$\rho(p) = -\frac{p^2 - ABp - B}{p^2 + CBp + B}$$

System response to a step function is

$$\Gamma(p) = \frac{\rho(p)}{p}$$

hence

$$\Gamma(p) = -\frac{1}{p}\left[\frac{p^2-ABp-B}{p^2+CBp+B}\right] = -\left[\frac{p}{(p+a)(p+b)} - \frac{AB}{(p+a)(p+b)} - \frac{B}{p(p+a)(p+b)}\right] \tag{10}$$

where a and b are the real negative roots† of the equation

$$p^2+CBp+B = (p+a)(p+b)$$

System response on the oscilloscope screen which is a sum of the incident and reflected waves can be obtained by the inverse Laplace transform of the elements of Eqn. (10)

† It can be shown that for real dielectrics $0<\varepsilon_\infty<\varepsilon_o$ always holds, so that $\frac{(CB)^2}{4} - B > 0$ and the roots are real.

$$f(t) = 1 + \Gamma(t) = 2 - e^{-at}\left[\frac{a^2+aAB-B}{a(a-b)}\right] + e^{-bt}\left[\frac{b^2+bAB-B}{b(a-b)}\right] \quad (11)$$

The behaviour of the system described by Eqn. (11) is represented by a simple equivalent circuit as shown in Fig. 6, where $Y = j\omega C = j\omega C_o \varepsilon_r^*(\omega) = j\omega C_o \varepsilon_\infty + \frac{j\omega C_o(\varepsilon_o - \varepsilon_\infty)}{1+j\omega\tau}$.

3.1.4 Dielectrics showing the Debye dispersion with distributed relaxation times

In this case, the permittivity is given as a superposition of terms of the form $\frac{A_i}{1+j\omega\tau_i}$, where A_i is the strength, and $A_i = \varepsilon_{o_i} - \varepsilon_\infty$, and τ_i is the relaxation time of the i^{th} term.

$$\varepsilon_r^* = \varepsilon_\infty + \sum_{i=1}^{n} \frac{A_i}{1+p\tau_i} \quad (12)$$

Substituting Eqn. (12) into Eqn. (2)

$$\rho(p) = \frac{1 - pC_oZ_o[\varepsilon_\infty + \sum_{i=1}^{n} \frac{A_i}{1+p\tau_i}]}{1 + pC_oZ_o[\varepsilon_\infty + \sum_{i=1}^{n} \frac{A_i}{1+p\tau_i}]}$$

$$= \frac{\sum_{i=1}^{n}(1+p\tau_i) - pC_oZ_o[\varepsilon_\infty \sum_{i=1}^{n}(1+p\tau_i) + \sum_{i=1}^{n} A_i]}{\sum_{i=1}^{n}(1+p\tau_i) + pC_oZ_o[\varepsilon_\infty \sum_{i=1}^{n}(1+p\tau_i) + \sum_{i=1}^{n} A_i]} \quad (13)$$

It is clear that the denominator of Eqn. (13) can be rearranged in increasing powers of p as:

$$1 + p[(\sum_{i=1}^{n}\tau_i) + C_oZ_o\varepsilon_\infty + (\sum_{i=1}^{n}\Delta\varepsilon_i)C_oZ_o]$$

$$+ p^2[\sum_{i=1}^{n}\tau_i \sum_{k=i+1}^{n}\tau_k + C_oZ_o\varepsilon_\infty(\sum_{i=1}^{n}\tau_i) + C_oZ_o \sum_{i=1}^{n}\Delta\varepsilon_i(\sum_{k=1}^{n}\tau_k)]$$

$$+ p^3[(\sum_{i=1}^{n}\tau_i \sum_{k=i+1}^{n}\tau_k \sum_{j=k+1}^{n}\tau_j) + C_oZ_o\varepsilon_\infty(\sum_{i=1}^{n}\tau_i \sum_{k=i+1}^{n}\tau_k)$$

$$+ C_oZ_o \sum_{i=1}^{n}\Delta\varepsilon_i(\sum_{\substack{k=1\\k\neq i}}^{n}\tau_k \sum_{\substack{j=k+1\\j\neq i}}^{n}\tau_j)]$$

$$+ \cdots\cdots\cdots\cdots\cdots\cdots\cdots\cdots\cdots$$

$$+ p^{n+1}(C_oZ_o\varepsilon_\infty \prod_{i=1}^{n}\tau_i)^\dagger$$

Hence, the step function response of the reflection coefficient is

$$\Gamma(p) = \frac{D(p)}{pR(p)} = \frac{D(p)}{q(p)}$$

where $D(p)$ and $R(p)$ are polynomials of degree $n+1$, but of different coefficients.

System response on the oscilloscope screen which is the sum of the incident and reflected waves can be obtained by the inverse Laplace transform and using Heaviside expansion formula

$$\Gamma(t) = 1 + \mathcal{L}^{-1}[\frac{D(p)}{q(p)}]$$

---

†Note the recurrence relations between the coefficient of the successive powers of p.

$$= 1 + \sum_{r=1}^{n+1} \frac{D(\alpha_r)}{q'(\alpha_r)} e^{\alpha_r t}$$

where α_r is the r^{th} root of the denominator and q' is the derivative of q with respect to p.

3.2 An alternative approach

System responses on the oscilloscope screen, for different dispersion mechanisms given in 3.1.1 through 3.1.4 are of considerable importance since they may be used for checking the experimental data so that necessary corrections can be easily provided (e.g., corrections for finite rise time of the system [12]). In addition, they may be used to calculate ε_o, ε_∞ and τ for the test substance by fitting the experimental data with the predicted curve by the method of least squares.

The main disadvantage of this type of approach is that the dispersion mechanism of a real dielectric is never exactly the same as one of the previously assumed types. This task is also complicated by the fact that we do not know in advance if time constants ought to be assumed in terms of either of these mechanisms. Therefore, the identification of the proper theoretical curve can only be obtained in an approximate way. In addition, there is a considerable amount of trial and error in this procedure.

In an alternative approach the relative permittivity

$\varepsilon_r^*(\omega)$ may be found directly by solving the Eqn. (2) for the real and imaginary parts of the relative permittivity.

$$\varepsilon_r'(\omega) = \frac{2|\rho(\omega)|\sin\,\theta(\omega)}{\omega C_o Z_o[(|\rho(\omega)|\cos\,\theta(\omega)\,+\,1)^2 + |\rho(\omega)|^2\sin^2\theta(\omega)]} \tag{14}$$

$$\varepsilon_r''(\omega) = \frac{(1\,-\,|\rho(\omega)|^2)}{\omega C_o Z_o[(|\rho(\omega)\ \cos\,\theta(\omega)\,+\,1)^2 + |\rho(\omega)|^2\sin^2\theta(\omega)]} \tag{15}$$

The reflection coefficient $\rho(\omega)$ appearing in Eqn. (14) and Eqn. (15) could be calculated by a discrete Fourier transform directly from the digitized system response f(t) displayed on the screen of the sampling oscilloscope. This technique was used in this task.

CHAPTER 4

UNCERTAINTY ANALYSIS

An important consideration in time domain metrology is the achievable accuracy. In this chapter, different contributions to the overall uncertainty in the permittivity measurement are discussed. In sections 4.1 to 4.3 possible systematic and random errors which could be present in the time domain techniques are discussed. These errors are divided into three types: incident waveform errors, sampling errors including noise, and time to frequency conversion errors.

Section 4.4 considers the conventional errors due to the mechanical accuracy in length measurement. In section 4.5 the fringing fields effect is studied and calculated. A correction factor to compensate for the measurement errors due to fringing fields is also provided.

4.1 Incident waveform errors

This category is limited to systematic errors in the analog waveforms before sampling. Measurement errors occur because the waveform incident upon the sample under test changes with time. Since the reflection coefficient is the ratio of the DFT of two waveforms measured at different times, one obvious source of error is a fluctuation in the generator output in the interval between the two readings of the incident and reflected waves. Changes have been observed with the solid state generator being used. However, the changes are so obvious that they are easy to spot and correct.

A more subtle reason for error is the imperfections in the connectors and transmission lines immediately adjacent to the sample under test, resulting in mismatch errors that cannot be time windowed out or removed by background subtraction. This type of error can be minimized by using precision air lines as sample holders (APC - 7 sample holder).

4.2 Sampling errors

This section examines sources of errors introduced between the analog input to the sampling head and the resultant digitized waveform. Smith [11] has given a detailed analysis of the translation of noise-like errors from time to frequency domain and derived expressions for noise upper bounds. In this section a brief discussion and tabulation of these errors, as well as the upper error bounds, will be given.

4.2.1 Time sampled errors

This is the error introduced in the frequency spectrum of a signal due to an error X_n in the measured time sample at time $t = nT$, that is

$$X_n = f(nT) - f_m(nT)$$

where $f_m(nT)$ is the measured value of the signal at $t = nT$.

Based on the assumption that X_n can be described as a real random variable with zero mean and variance σ_n^2, a quantity ξ which is an upper bound on the probability that a computed white-noise ordinate will exceed a quantity ε_N is given by

$$\varepsilon_N = T\sqrt{2N\sigma_N^2} \quad \mathrm{erf}^{-1}[\sqrt{1-\xi}] \tag{16}$$

where N is the number of time domain samples, T is the equivalent sampling interval and σ_N^2 is the variance of the sampled voltage due to the amplifier noise.

4.2.2 Time jitter error

If the scanning voltage is held fixed corresponding to a fixed point on the waveform being measured, the measured voltage will fluctuate because of imprecise triggering as the gate moves around over a small time segment about its mean position. This is called timing jitter. In other words, time jitter error is due to the uncertainty in the time location of the samples. The error voltage generated by timing jitter at a point is proportional to the slope of the waveform at that point.

Assuming that the timing errors are random, and that the slope is always essentially constant over the range of timing jitter, a quantity ξ which is an upper bound on the probability that the time jitter error in any frequency ordinate will exceed ε_T may be given by

$$\varepsilon_T = \left(\frac{T\sigma_T^2}{N}\right)^{\frac{1}{2}} \left(\int_{-\pi/T}^{\pi/T} |F(\omega)|^2 d\omega\right)^{\frac{1}{2}} \mathrm{erf}^{-1}[(1-\xi)] \text{ V-sec} \qquad (17)$$

where σ_T^2 is the variance of the time jitter.

4.2.3 Quantization error

This error is caused by converting the amplitude of the time response to numerical form. This usually requires that the range of amplitude values be divided into a finite set of equal increments, and all of the amplitudes which fall within the same interval are assigned the same numeric value. It is clear that such a system of measurement will cause an error, called quantization error, which can be no longer than the size of the interval used. If d is the quantization interval, an error up to $\pm \frac{d}{2}$ may occur in each time sample due to quantization.

Based on the assumption that the error voltage is with equal probability at any value within this interval, and that the signal changes through many successive quantization intervals between samples so that the successive errors are uncorrelated, then the error voltage is a random variable with a rectangular probability distribution, and variance

$$\sigma_q^2 = \frac{d^2}{12} \tag{18}$$

Substituting Eqn. (18) into Eqn. (16) we obtain an expression for the quantity ξ, which is an upper bound on the probability that the quantization error in any frequency ordinate will exceed ε_q

$$\varepsilon_q = Td\sqrt{N/6}\ \mathrm{erf}^{-1}[\sqrt{1-\xi}] \tag{19}$$

4.2.4 Amplitude jitter error

This error is due to the changes in a signal amplitude from sample to sample while the shape of the signal remains essentially unchanged. The signal may be expressed in the form

$$f_m(nT) = (1+a_n)\ f_m(nT)$$

where a_n is the amplitude jitter. If a_n is assumed to be a zero-mean normal random variable which is independent of the amplitude jitter at any other time sample, the error in the spectrum then becomes

$$\varepsilon_a = \sigma_a \left(\frac{T}{\pi} \int_{-\pi/T}^{\pi/T} |F(\omega)|^2 d\omega\right)^{\frac{1}{2}} \operatorname{erf}^{-1}[\sqrt{1-\xi_a}] \qquad (20)$$

Eqn. (20) gives the error bound in terms of the confidence level ξ_a.

4.2.5 Additive Gaussian noise

This is the error in the spectrum of a signal due to zero mean additive Gaussian noise. The resulting error spectrum will be given by

$$Z_n(\omega) = - \sum_{n=0}^{N-1} TX(nT)\ e^{-j\omega nT}$$

where X(t) is a stationary Gaussian process. In the case of uncorrelated noise from sample to sample (white noise), the error bound due to additive noise, ε_ω, is given by [11]

$$\varepsilon_\omega = \sqrt{2N}\ T\ \sqrt{R(\tau)}\ \operatorname{erf}^{-1}[\sqrt{1-\xi_n}] \qquad (21\text{-a})$$

$$\varepsilon_\omega = \sqrt{2N}\ T\ \left(\frac{1}{2\pi} \int_{-\infty}^{\infty} S(\omega) d\omega\right)^{\frac{1}{2}} \operatorname{erf}^{-1}[\sqrt{1-\xi_n}] \qquad (21\text{-b})$$

where $S(\omega)$ is the power density spectrum of the noise. Equation (21-b) follows from Eqn. (21-a) since $S(\omega)$ and $R(\tau)$ are Fourier transform pairs.

4.2.6 Combined errors from noise-like sources

So far we have considered the contribution to the errors from noise-like sources separately. If we use the same confidence level, ξ, for each individual bound, we find the combined bound to be

$$\varepsilon_c = (\varepsilon_q^2 + \varepsilon_a^2 + \varepsilon_T^2 + \varepsilon_N^2)^{\frac{1}{2}}$$

4.3 Time to frequency conversion errors

Aliasing and truncation errors are the major sources of error in estimating the spectrum of the continuous time domain waveform from its N sampled values.

4.3.1 Aliazing error

Aliazing error is an error introduced in the spectrum of a signal caused by representing the continuous signal by a uniform train of samples. Let us suppose that we form the signal spectrum from its time sampled values, $f(nT)$, at time $t = nT$, where T is the sampling interval. This is done by using the formula

$$F_s(\omega) = \sum_{n=-\infty}^{\infty} T\, f(nT)e^{-j\omega nT} \qquad (22)$$

which approximates the Fourier integral

$$F(\omega) = \int_{-\infty}^{\infty} f(t)e^{-j\omega t}\, dt$$

Eqn. (22) may also be written as [16]

$$F_s(\omega) = \sum_{l=-\infty}^{\infty} F(\omega + \frac{2\pi l}{T})$$

The computed spectrum is thus periodic, recurring at angular frequency interval $\frac{2\pi}{T}$, the sampling frequency. In particular, over the region $-\omega_N$ to ω_N , where $\omega_N = \frac{\pi}{T}$ is defined as the Nyquist frequency, $F_s(\omega)$ equals the required spectrum $F(\omega)$ plus unwanted contributions from the adjacent lobes of the "aliases" of $F(\omega)$ at $F[\omega \pm \frac{2\pi}{T}]$, $F[\omega \pm \frac{4\pi}{T}]$, etc.

Practically, the aliasing error may be reduced by making the Nyquist frequency as large as possible, thus spacing adjacent lobes further apart.

4.3.2 Truncation error

A truncation error occurs because all samples beyond the N^{th} sample are not considered in the computing spectrum Eqn. (22), i.e.,

$$F_{error}(\omega) = \sum_{n=N}^{\infty} T\, f(nT) e^{-j\omega nT} \tag{23}$$

This error is minimized, in signals of limited time responses, by making the time window NT large enough so the network responses have negligible magnitude outside it.

When the signal has the form of a step, a large truncation error results when only a finite number of samples is used. The correct waveform, however, may be represented by N samples for the initial rising part of the step, followed by an infinite number of almost equal samples representing the tail, the slow decay given the form $e^{-\alpha t}$, where $\alpha \to 0$. Then, the spectrum of the step is

$$A^*(\omega) = T \sum_{n=0}^{N-1} f(nT)e^{-jnT\omega} + T\ f(NT) \sum_{n=N}^{\infty} e^{-jnT\omega} \cdot e^{-\alpha(n-NT)}$$

The second summation has the form, as $\alpha \to 0$

$$\frac{e^{-jNT\omega}}{1-e^{-jT\omega}}$$

Therefore,

$$A^*(\omega) \approx T \sum_{n=0}^{N-1} f(nT)e^{-jnT\omega} + T \frac{f(NT)e^{-jNT\omega}}{1-e^{-jT\omega}}$$

It is the second term in the above equation that is lost due to truncation. Thus, when the spectrum of a step is being computed, the following component is added at each ordinate $F(\omega)$

$$Tf(NT) \frac{e^{-j(N-\frac{1}{2})T\omega}}{e^{\frac{jT\omega}{2}} - e^{-\frac{jT\omega}{2}}} = \frac{T\ f(NT)}{2\ \sin(\frac{\omega T}{2})}\ e^{-j(N-\frac{1}{2})\omega T} e^{-j(\frac{\pi}{2})} \qquad (24)$$

In the computer program which evaluates the continuous Fourier transform, the input parameter KIND is normally zero; when set to -1, the step correction in Eqn. (24) is applied.

Summary of the results: The major conclusions of the analysis given in [11] are presented in Table 3. For noise-like errors it is seen that an amplitude level ε may be found in each case, such that the probability of its being exceeded is not greater than ξ.

4.4 Overall uncertainty in permittivity measurement

In this section systematic uncertainties in the characteristic impedance of the coaxial line and the air capacitance of the test capacitor, due to the mechanical accuracy in length measurement, are discussed.

The relationship between the uncertainty interval for the different contributions and the uncertainty intervals for the measured real and imaginary parts of the complex permittivity is presented. This relation gives the same odds for each of the variables and for the result.

Uncertainties due to the mechanical inaccuracy in length measurement: The characteristic impedance of a coaxial line is determined according to its physical dimensions. Accordingly, any uncertainty in length measurement will cause an error in the characteristic impedance of the line. For modern coaxial components the uncertainty in length measurement may be assumed to be 0.1%. Therefore, for the 50 Ω coaxial line, the uncertainty ΔZ_o may be

ERROR	CONDITIONS	BOUND
Aliasing	$\lvert F(\omega)\rvert \le \frac{A}{\omega^2}$ $\lvert\omega\rvert \ge \omega_N$	$\frac{AT^2}{4}$
	$\lvert F(\omega)\rvert$ is monotonically decreasing for $\lvert\omega\rvert \ge \omega_N$	$2\lvert F(\omega_N)\rvert + \frac{1}{\omega_N}\int_{\omega_N}^{\infty} \lvert F(\omega)\rvert d\omega$
Truncation	$\lvert f(t)\rvert \le Ae^{-\alpha T}$ $t \ge NT$	$\frac{ATe^{-\alpha NT}}{1-e^{-\alpha T}} \le \left[1 + \frac{1}{\alpha T}\right] ATe^{-\alpha NT}$
	$\lvert f(t)\rvert$ is monotonically decreasing for $t \ge NT$	$T\, f(NT) + \int_{NT}^{\infty} \lvert f(t)\rvert dt$
Quantization	d = quantization interval	$\epsilon_q = T\, d\sqrt{\frac{N}{6}}\, \mathrm{erf}^{-1}\, [\sqrt{1 - \xi}]$
Amplitude Jitter	σ_a^2 = variance of amplitude jitter	$\epsilon_a = \sigma_a\sqrt{\frac{T}{\pi}\int_{-\pi/T}^{\pi/T} \lvert F(\omega)\rvert^2 d\omega}\, \mathrm{erf}^{-1}\, [\sqrt{1 - \xi}]$
		$\epsilon_a \le \sqrt{2}\, \sigma_a\, F_{max}\, \mathrm{erf}^{-1}\, [\sqrt{1 - \xi}]$
Time Jitter	σ_τ^2 = variance of time jitter	$\epsilon_\tau = \sigma_\tau\sqrt{\frac{T}{\pi}\int_{-\pi/T}^{\pi/T} \omega^2 \lvert F(\omega)\rvert^2 d\omega}\, \mathrm{erf}^{-1}\, [\sqrt{1 - \xi}]$
		$\epsilon_\tau \le \sqrt{\frac{2}{3}}\, \sigma_\tau \left(\frac{\pi}{T}\right) F_{max}\, \mathrm{erf}^{-1}\, [\sqrt{1 - \xi}]$
White Noise	$R(\tau)$ = autocorrelation of the noise $S(\omega)$ = power density	$\epsilon_W = \sqrt{2N}\, T\sqrt{R(o)}\, \mathrm{erf}^{-1}\, [\sqrt{1 - \xi}]$
		$\epsilon_W = \sqrt{2N}\, T\sqrt{\frac{1}{2\pi}\int_{-\infty}^{\infty} S(\omega) d\omega}\, \mathrm{erf}^{-1}\, [\sqrt{1 - \xi}]$
Combined Noise-Like Sources		$\epsilon_c = \sqrt{\epsilon_q^2 + \epsilon_a^2 + \epsilon_\tau^2 + \epsilon_W^2}$

$\omega_N = \frac{\pi}{T}$ = Nyquist frequency.

T = sampling interval.

N = number of samples.

ξ = confidence level (i.e., upper bound on probability that the amplitude error will exceed a quantity ϵ).

F_{max} = maximum of $\lvert F(\omega)\rvert$ for $\lvert\omega\rvert \le \omega_N$.

TABLE 3 ERROR BOUNDS

assumed to be equal to 0.1 Ω (typical value for APC-7 coaxial connectors [17]).

The uncertainty ΔC_o in the air capacitance of the test capacitor results also from the uncertainty in the dimensions measurement. The dimensions of the parallel plate capacitor can be measured within an accuracy of 0.1%, consequently the calculated uncertainty in the air capacitance of the test capacitor will be 3×10^{-14} Farad.

The overall uncertainty: So far we studied the individual contributions to the overall uncertainty in the permittivity measurement. The following summarizes the different contributions to the overall uncertainty:

$\Delta|\rho|$ and $\Delta\theta$ - the uncertainties in the modulus and phase of the reflection coefficient. These uncertainties are caused by the noise-like errors in the TDR system (in time domain) and by the time to frequency conversion errors.

ΔZ_o - the uncertainty in the characteristic impedance of the transmission line, which may be essentially due to the mechanical inaccuracy in the dimensions measurement.

ΔC_o - the uncertainty in the air capacitance of the test capacitor. This is also due to the uncertainty in the dimensions measurement.

It is the uncertainties in the real and imaginary parts of the complex permittivity that are required. Therefore, it is necessary to determine how these individual uncertainties propagate into the results.

The relation between the uncertainty interval for the different contributions and the uncertainty intervals for the resultant real and imaginary parts of the complex permittivity, which gives the same odds for each of the variables and for the result, is [19]:

$$\Delta\varepsilon' = [(\frac{\partial\varepsilon'}{\partial C_o}\Delta C_o)^2 + (\frac{\partial\varepsilon'}{\partial Z_o}\Delta Z_o)^2 + (\frac{\partial\varepsilon'}{\partial\rho}\Delta\rho)^2 + (\frac{\partial\varepsilon'}{\partial\theta}\Delta\theta)^2]^{\frac{1}{2}} \qquad (26)$$

$$\Delta\varepsilon'' = [(\frac{\partial\varepsilon''}{\partial C_o}\Delta C_o)^2 + (\frac{\partial\varepsilon''}{\partial Z_o}\Delta Z_o)^2 + (\frac{\partial\varepsilon''}{\partial\rho}\Delta\rho)^2 + (\frac{\partial\varepsilon''}{\partial\theta}\Delta\theta)^2]^{\frac{1}{2}} \qquad (27)$$

The partial derivatives appearing in Eqn. (26) and Eqn. (27) are given by

$$\frac{\partial\varepsilon'}{\partial C_o} = - \frac{2|\rho|\sin\theta}{\omega C_o{}^2 Z_o\{(|\rho|\cos\theta+1)^2 + |\rho|^2\sin^2\theta\}}$$

$$\frac{\partial\varepsilon'}{\partial Z_o} = - \frac{2|\rho|\sin\theta}{\omega C_o Z_o{}^2\{(|\rho|\cos\theta+1)^2 + |\rho|^2\sin^2\theta\}}$$

$$\frac{\partial\varepsilon'}{\partial|\rho|} = \frac{2(1-|\rho|^2)\sin\theta}{\omega C_o\ Z_o\{(|\rho|\cos\theta+1)^2 + |\rho|^2\sin^2\theta\}^2}$$

$$\frac{\partial\varepsilon'}{\partial\theta} = \frac{2|\rho|\{(1+|\rho|^2)\cos\theta + 2|\rho|\}}{\omega C_o\ Z_o\{(|\rho|\cos\theta+1)^2 + |\rho|^2\sin^2\theta\}^2}$$

$$\frac{\partial \varepsilon''}{\partial C_o} = - \frac{(1-|\rho|^2)}{\omega C_o^2 Z_o\{(|\rho|\cos\theta+1)^2 + |\rho|^2\sin^2\theta\}}$$

$$\frac{\partial \varepsilon''}{\partial Z_o} = - \frac{(1-|\rho|^2)}{\omega C_o Z_o^2\{(|\rho|\cos\theta+1)^2 + |\rho|^2\sin^2\theta\}}$$

$$\frac{\partial \varepsilon''}{\partial |\rho|} = - \frac{2\{2|\rho| + (1+|\rho|^2)\cos\theta\}}{\omega C_o Z_o\{(|\rho|\cos\theta+1)^2 + |\rho|^2\sin^2\theta\}^2}$$

$$\frac{\partial \varepsilon''}{\partial \theta} = \frac{2|\rho|(1-|\rho|^2)\sin\theta}{\omega C_o Z_o\{(|\rho|\cos\theta+1)^2 + |\rho|^2\sin^2\theta\}^2}$$

Equations (26) and (27) might be used directly as an approximation for calculating the uncertainty intervals in ε' and ε''.

4.5 Fringing fields effect

In the proposed technique a small shunt capacitor terminating a coaxial line section is used as a sample holder. However, the equivalent circuit shown in Fig. 4(b) is not absolutely correct because of fringing fields effect. In this section we will discuss these fringing effects and a correction factor will be provided.

Green [18] in treating some important transmission line problems found a relevant numerical solution by solving Laplace's equation in cartesian coordinates. The results of this numerical solution are in good agreement with the calculated values, using the small aperture technique, given by Marcuvitz [20].

This problem consists of a coaxial cavity closed at one end with a conducting cover plate from which the inner conductor is shorted by a gap of width $\frac{S}{2}$, as shown in Fig. 7(a). In reference to the plane T, the inner conductor is shown to be terminated to ground through a capacitance C, Fig. 7(b).

$$C = \frac{\pi a^2 \varepsilon}{2S} + \frac{2a\varepsilon}{\ln \frac{b-a}{S}} \tag{25}$$

This formula is said to be valid under the restrictions

$$\lambda >> b-a$$

$$S << b-a$$

and can be seen to consist of two distinct parts, a component giving the parallel plate capacity between the inner conductor and the cover plate and a "fringing" term.

It is of interest to see numerical values of the fringing capacitance relative to a given value of the parallel plate capacitance. Equation (25) has been programmed and the parallel plate capacitance, C_p, the fringing capacitance, C_f, and the ratio C_f/C_p have been

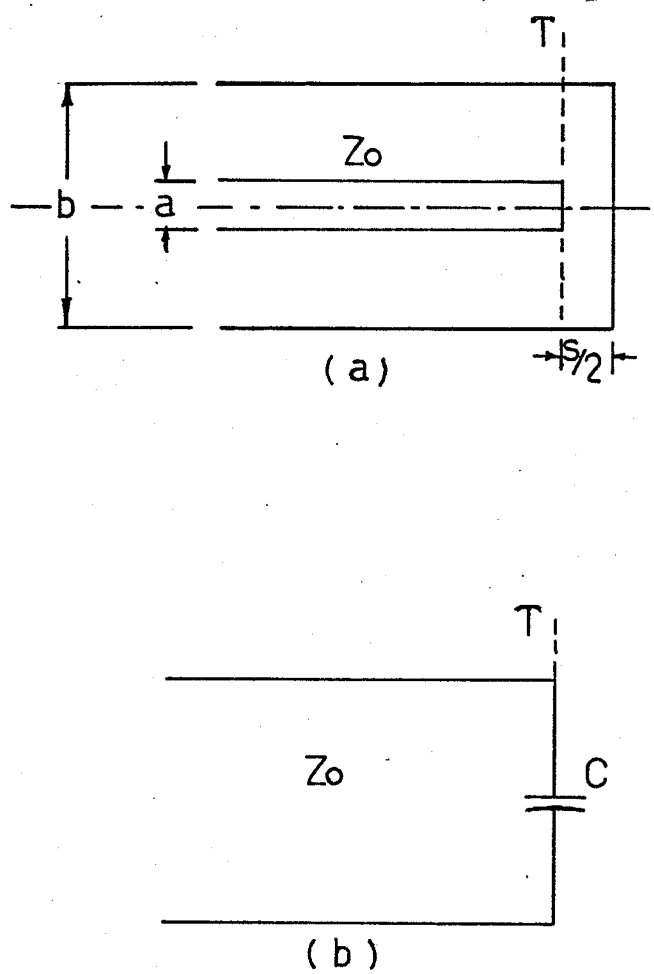

Fig 7 Marcuvitz problem
(a) Cavity with foreshortened inner conductor. (b) Equivalent circuit.

Table 4

Fringing Fields Effect

C_p* (parallel plate capacitance)	C_f (fringing capacitance)	$C_R=C_f/C_p$%	S/2 (gap width)
	A** = 6.0 mm		
12.50	0.020	0.16	20 μm
8.30	0.022	0.26	30 μm
6.25	0.023	0.37	40 μm
5.00	0.024	0.48	50 μm
4.20	0.025	0.61	60 μm
3.60	0.026	0.73	70 μm
3.10	0.027	0.87	80 μm
2.80	0.028	1.0	90 μm
	A = 6.2 mm		
10.70	0.022	0.2	25 μm
8.90	0.0225	0.25	30 μm
7.60	0.023	0.30	35 μm
6.70	0.024	0.36	40 μm
5.90	0.0245	0.41	45 μm
5.30	0.025	0.47	50 μm
4.90	0.0257	0.53	55 μm
4.10	0.0268	0.65	65 μm
3.10	0.0286	0.91	40 μm
	A = 8.0 mm		
11.1	0.033	0.29	40 μm
8.9	0.035	0.39	50 μm
7.4	0.036	0.49	60 μm
6.3	0.0376	0.59	70 μm
5.6	0.039	0.70	80 μm
4.9	0.040	0.82	90 μm
4.0	0.043	1.00	0.11 mm
3.2	0.046	1.45	0.14 mm
	A = 10 mm		
11.6	0.050	0.44	60 μm
9.9	0.053	0.53	70 μm
7.7	0.057	0.74	90 μm
6.3	0.061	0.97	0.11 mm
5.3	0.065	1.21	0.13 mm
5.0	0.066	1.34	0.14 mm
4.1	0.072	1.7	0.17 mm
3.3	0.078	2.37	0.21 mm

* Capacitances are in pico-Farads.
** A is the diameter of the inner conductor.

computed for given, different, inner conductor diameters and the gap width was taken as a running parameter. The results are shown in Table 4.

Table 4 shows that increasing the diameter of the inner conductor is not advisable. It is true that increasing the diameter of the inner conductor makes the ratio C_f/C_p smaller for the same gap width. For capacitance values of practical interest, however, increasing the diameter of the inner conductor makes the ratio C_f/C_p larger. Table 4 also shows that the fringing capacitance is of the order of 0.3×10^{-13} Farads for the values of C_p of practical interest.

One of the basic assumptions in this work is that $C(p) = C_o \varepsilon_r^*(p)$. This equation assumes direct proportionality between C_o and $C(p)$ which is not absolutely correct because of the fringing fields effect. Having an idea about the value of fringing capacitance, it is of interest to derive a correction factor to compensate for the error in ε' and ε'' due to fringing fields.

The actual relation may be assumed to be of the form

$$C(p) = A\varepsilon_r^* + B$$

where A is the part of the total capacitance filled with the dielectric under test (basically the parallel plate capacitance, and part of the fringing capacitance due to the meniscus), and B is the remaining part of the fringing capacitance. Substituting C(p) into Eqn. (1) we obtain

$$\rho(p) = \frac{1 - Z_o p(A\varepsilon_r^* + B)}{1 + Z_o p(A\varepsilon_r^* + B)}$$

$$\rho(p) = \frac{1 - Z_o pA(\varepsilon_r^* + \frac{B}{A})}{1 + Z_o pA(\varepsilon_r^* + \frac{B}{A})} \tag{28}$$

Solving for ε_r^*

$$\varepsilon_r^* + \frac{B}{A} = \frac{1}{pZ_oA}\left(\frac{1-\rho}{1+\rho}\right)$$

Substituting

$$\varepsilon_r^* = \varepsilon' - j\varepsilon'', \text{ and } p = j\omega$$

Then

$$\varepsilon' - j\varepsilon'' + \frac{B}{A} = \frac{1}{j\omega Z_oA}\left(\frac{1-\rho}{1+\rho}\right)$$

$$= \frac{-j}{\omega Z_oA}\left(\frac{1-|\rho|^2 + 2j|\rho|\sin\theta}{(1+|\rho|\cos\theta)^2 + |\rho|^2\sin^2\theta}\right)$$

$$\varepsilon' + \frac{B}{A} = \frac{2|\rho|\sin\theta}{\omega Z_oA[(1+|\rho|\cos\theta)^2 + |\rho|^2\sin^2\theta]} \tag{29}$$

$$\varepsilon'' = \frac{(1-|\rho|^2)}{\omega Z_oA[(1+|\rho|\cos\theta)^2 + |\rho|^2\sin^2\theta]} \tag{30}$$

It is clear from Eqn. (29) and Eqn. (30) that the value of ε' calculated in the frequency domain from the data transformed from the time domain measurements is larger than the true value by a factor equal to $\frac{B}{A}$, while ε'' has the correct value.

The following example illustrates this conclusion. Consider a dielectric of the Debye type:

$$\varepsilon_r^* = \varepsilon_\infty + \frac{\varepsilon_o - \varepsilon_\infty}{1+p\tau}$$

Substituting ε_r^* into Eqn. (28)

$$\rho(p) = \frac{1 - Z_o pA(\varepsilon_\infty + \frac{\varepsilon_o - \varepsilon_\infty}{1+p\tau} + \frac{B}{A})}{1 + Z_o pA(\varepsilon_\infty + \frac{\varepsilon_o - \varepsilon_\infty}{1+p\tau} + \frac{B}{A})}$$

$$= \frac{1 - Z_o pA(\varepsilon'_\infty + \frac{\varepsilon'_o - \varepsilon'_\infty}{1+p\tau})}{1 + Z_o pA(\varepsilon'_\infty + \frac{\varepsilon'_o - \varepsilon'_\infty}{1+p\tau})} \tag{31}$$

where $\varepsilon'_\infty = \varepsilon_\infty + \frac{B}{A}$ and $\varepsilon'_o = \varepsilon_o + \frac{B}{A}$. From Eqn. (31) it is clear that the time response displayed on the oscilloscope screen will be for a dielectric of Debye dispersion, Eqn. (11) with the modified parameters ε'_∞ and ε'_o. Since both ε'_o and ε'_∞ are shifted by a quantity $\frac{B}{A}$ it is concluded that ε' will be shifted by a value of $\frac{B}{A}$. ε'' on the other hand, will not include any error due to fringing fields effect because it depends on the difference between ε_o and ε_∞.

CHAPTER 5

MEASUREMENT SYSTEM

COMPONENTS AND UNCERTAINTY CALCULATIONS

In Chapter 4, the different contributions to the uncertainties in the real and imaginary parts of the complex permittivity have been studied. The overall uncertainties are shown to be obtained from Eqn. (25) and (26), which require predetermination of the individual uncertainty interval for each of the different variables.

The determination of ΔZ_o and ΔC_o can be easily obtained from the physical dimensions of the coaxial components used (4.4); uncertainties in $\Delta|\rho|$ and $\Delta\theta$, on the other hand, are caused by the noise-like errors in the TDR system and by the time to frequency conversion errors (4.2 and 4.3). These errors, however, are dependent on the measurement system components and also require *a priori* knowledge of the measured waveforms. Therefore, the first part of this chapter will describe briefly the measurement system components. In section 4.2, the upper bounds of the noise-like errors as well as the overall uncertainties in ε' and ε'' have been calculated. Section 4.3 describes an attempt to choose the optimum value of the capacitance to be used for a specified frequency band.

5.1 Measurement system components

A block diagram of the measurement system is illustrated in Fig. 8. The system is shown in simplified form to clearly indicate the interconnection of the four essential parts: step function generator, sampling system and X-Y recorder, temperature control chamber, and the APC-7 coaxial line as sample holder.

A brief description of the system parts follows.

5.1.1 Step function generator

The Hewlett-Packard model 1106A tunnel-diode pulse generator mount connects directly to the remote sampler for TDR system. The amplitude of the generated step is greater than 200 mV into 50 Ω line, with a rise time of 20 psec, approximately. The mount output impedance is 50 ± 2% Ω.

5.1.2 Sampling system and X-Y recorder

The sampling system consists of:

Model HP 1817A remote sampler, which is a single channel, 50 Ω feed-through sampler. The remote sampler provides bias and trigger signals for operating tunnel-diode pulse generator when used as a time-domain reflecto-

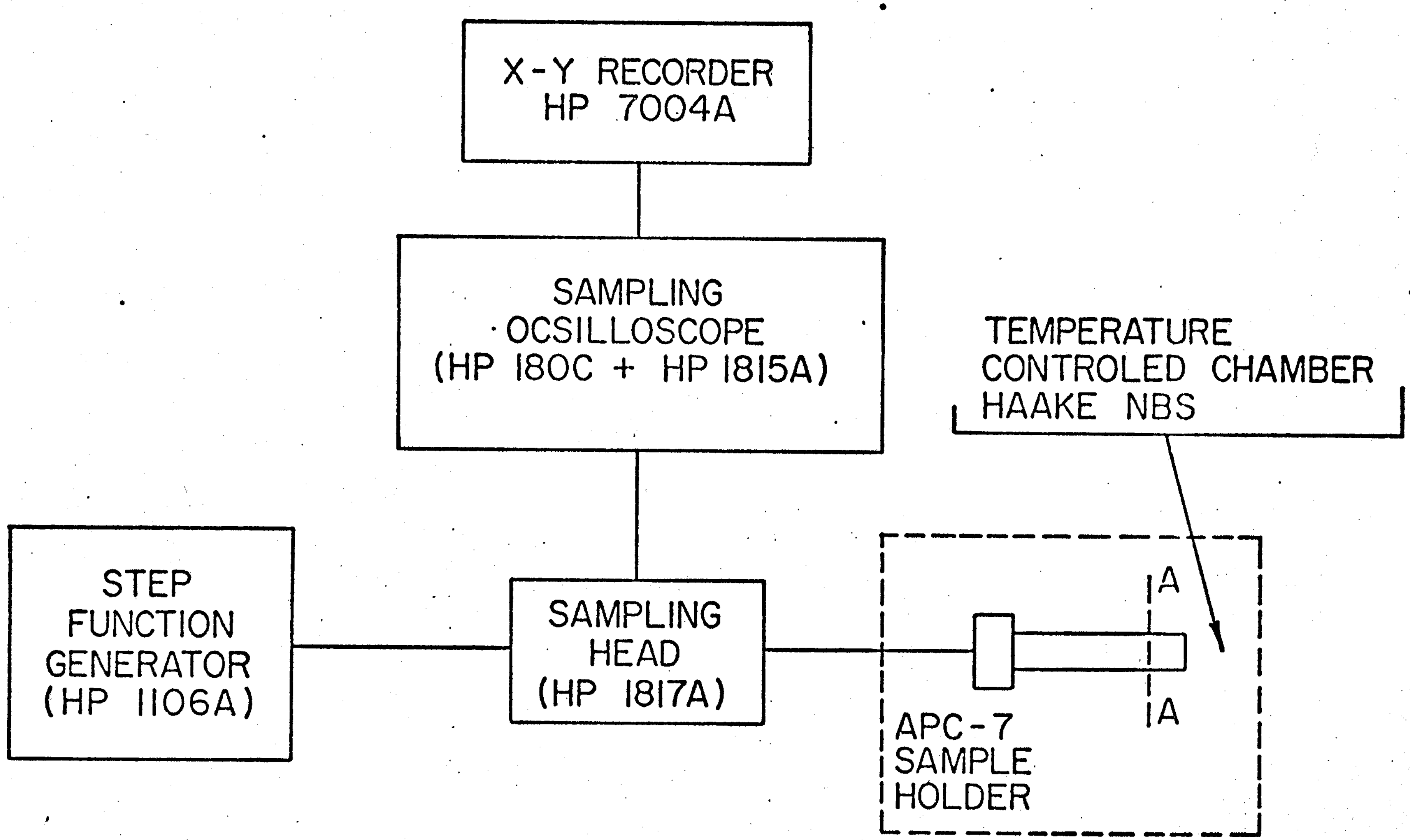

Fig.8 Experimental set_up.

meter. The system rise time is less than 35 psec incident as measured with model 1106A tunnel diode. The maximum safe input voltage is 1 volt.

Model HP 180 C Oscilloscope and Model HP 1815 TDR Plug-in. The model HP 1815 TDR plug-in provides the drive voltages for the oscilloscope horizontal amplifiers to position each sample dot on the CRT. In vertical axis the TDR takes samples of the incoming signals and supplies the drive voltages directly to the oscilloscope CRT. In addition model 1815 provides the required blanking pulses to the CRT. A marker pulse is supplied to the control grid of the CRT to intensify the presentation of one dot. The calibrated TDR system allows analysis of broad band microwave components, identifying discontinuities as close as 0.25 inch apart.

The sampling oscilloscope is mainly used as an analog sample and hold circuit with about a 30 psec sample time. This allows a transient response with microwave frequency components to be examined point by point. Waveforms displayed on the scope face provide a convenient quick check that the main and reference signals are in their proper positions and indicate gross discrepancies before the scanning begins.

X-Y Recorder (Model HP 7004 A). Displays are recorded on X-Y recorder using signals available on the recorder output connectors on the rear of the oscilloscope.

The horizontal voltage is available on the MAIN SWEEP OUTPUT terminal and the vertical voltage is available on the DELAYED GATE OUTPUT terminal. The RECORDER or MANUAL positions of the SCAN switch are used for obtaining X-Y plots. With the SCAN switch on RECORD position, one automatic recorder sweep starts. The recording cycle is complete after approximately 60 seconds. The sensitivity of the recorder outputs are approximately 100 mV/CRT DIV.

5.1.3 Temperature control

A temperature controlled chamber (HAAKE NBS circulator) has been used to keep the sample at constant, defined temperature. The standard thermoregulator in the circulator is suitable for operation in the range from 0° to 100°C. For other ranges, we can select contact and control thermometers which are suitable for the desired range between -60° and 350°C.

Normally, this circulator cannot be used for control below approximately 45°C without providing additional cooling facilities. The reason for this is that both pumping friction and the motor add some heat to the insulated bath. For continuous low temperature work below ambient down to -20°C, the mechanical refrigeration unit KR30 was used, which offers a considerably fast pull down time due to the strong built-in ¼ H.P. compressor. This instrument does not have a built-in circulating pump so that the liquid has to be circulated through its coil system and the heat exchanger chamber by aid of the circulator pump. The sample temperature is measured by a thermocouple fed to the model HP 3440 A digital voltmeter.

5.2 Typical waveform calculations

Since *a priori* knowledge of the waveforms is required, for certain cases, for the estimation of the noise-like errors bounds, a typical experimental result for the alkyl alcohol $C_8H_{17}OH$ at 25°C will be considered. Figure 9 shows the amplitude spectra of the reflection coefficient.

The following are the uncertainty intervals, calculations in the modulus and phase of the reflection coefficient, using the measurement set-up described in section 5.1 and for the typical waveform of Fig. 9.

(a) The amplitude level of white noise exceeded with a probability ξ is given by

$$\varepsilon_N = T\sqrt{2N\sigma_V^2}\,\mathrm{erf}^{-1}(\sqrt{1-\xi})$$

and for $\xi = 1\%$

$$\xi_{1,N} = 1.99T\sqrt{2N\sigma_V^2}$$

For the tunnel diode pulse generator at 100 KHz, and for 10 mV/cm oscilloscope sensitivity, the noise standard deviation is 6 mV [11].

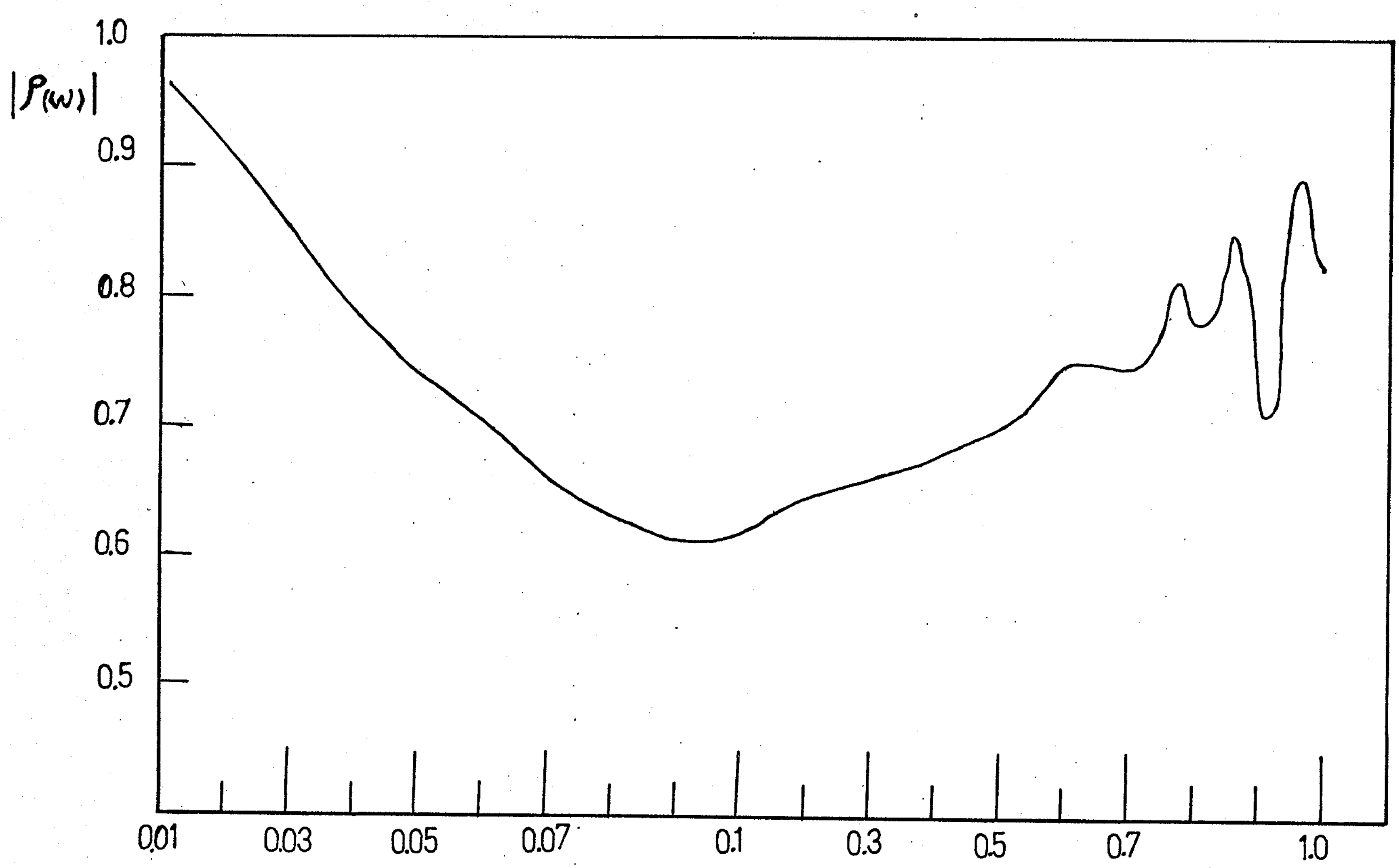

Fig.9 Amplitude spectra of the reflection coefficient of $C_8H_{17}OH$ alkyl alcohol at 25°C.

For N = 250 and T = 0.1 nsec

$$\varepsilon_{1,N} = 1.99 \times 0.1\sqrt{2 \times 250 \times 36} \times 10^{-3}$$
$$= 26.3 \times 10^{-3} \text{ volt-nsec}$$

(b) For time jitter, the amplitude level exceeded with a probability of 1% is given by

$$\varepsilon_{1,j} = 1.99\ \sigma_T \left(\frac{T}{\pi} \int_{-\pi/T}^{\pi/T} \omega^2 |F(\omega)|^2\, d\omega\right)^{\frac{1}{2}}$$

From Fig. 9 the value of $|\rho(\omega)|$ may be taken as 0.8 from f =0.01 GHz to 1 GHz which is the frequency range of interest and zero elsewhere. For the 12 GHz oscilloscopes the standard deviation σ_T was 1.9 psec (Appendix 1). Substituting these values with T = 0.1 nsec and N = 250

$$\varepsilon_{1,j} = 1.99 \times 1.9 \times 4 \times 10^{-3} \left(\frac{0.1}{\pi}\left[\frac{\omega^3}{3}\right]_{2\pi \times 0.01}^{2\pi}\right)^{\frac{1}{2}}$$
$$= 34.72 \times 10^{-3} \text{ volt-nsec}$$

(c) Since the amplitude jitter is not measurable [11], taking the above σ_V, we may substitute into the amplitude jitter expression for 1% probability, Table 3.

$$\varepsilon_{1,A} = 1.99 \times 6 \times 10^{-3} \left(\frac{0.1}{\pi}[\omega]_{2\pi\times0.01}^{2\pi}\right)^{\frac{1}{2}} \times 4$$

$$\simeq 31 \times 10^{-3} \text{ volt-nsec}$$

The resultant upper bound of the combined noise-like error sources

$$\varepsilon_{1,Res} = \sqrt{\Sigma\varepsilon_r^2} = 53.5 \times 10^{-3} \text{ volt-nsec}$$

which corresponds to an uncertainty in the magnitude of the reflection coefficient of ≃ 1.4%, and an uncertainty of the phase angle of 0.8°. Similar calculations have been performed for the frequency range from 0.01 to 3 GHz. In this case the modulus of the reflection coefficient, $|\rho(\omega)|$, was assumed to be 0.8 in the specified frequency range and zero elsewhere. The resultant uncertainties in the magnitude and phase of the reflection coefficient are 4.7% and 2.7°, respectively, which are quite large and so the measurements in this frequency band necessitate some waveform stabilization procedures.

It is the uncertainties in the real and imaginary parts of the complex permittivity that are required. The following paragraphs will describe a method designed to estimate the uncertainties in permittivity measurement.

A computer program to compute the uncertainties in ε' and ε'' due to the maximum expected error in the modulus of the reflection coefficient, which clearly occurs at zero error in the phase angle, was written that requires as inputs:

(1) The frequency at which the uncertainties are to be computed.

(2) The values of ε' and ε'' at each frequency.

(3) The estimated error in the modulus of the reflection coefficient.

A similar program to compute the uncertainties in ε' and ε'' due to the maximum expected error in the phase angle of the reflection coefficient, which clearly occurs at zero error in the modulus, was written which requires the same input data. The results of these computations are shown in Fig. 10. Figure 10 shows that the uncertainties $\Delta|\rho|$ and $\Delta\theta$ contribute to the errors in ε' and ε'' measurements both at the frequency band boundaries and in the relaxation region.

To calculate the overall uncertainties in ε' and ε'' a computer program to calculate $f\Delta\varepsilon'$ and $f\Delta\varepsilon''$ (from Eqn. (26) and Eqn. (27)) was written requiring as inputs:

(1) Typical values of the test capacitor and the characteristic impedance of the transmission line.

(2) The assumed uncertainties in the specified frequency range, ΔC_o, ΔZ_o, $\Delta|\rho|$ and $\Delta\theta$.

(3) Initial, final, and incremental values of $f\varepsilon'$ which is the running parameter, and some specified values of $f\varepsilon''$ of practical interest.

Figures (11) and (12) show the results of the numerical solutions of Eqn. (26) and Eqn. (27) for the typical values

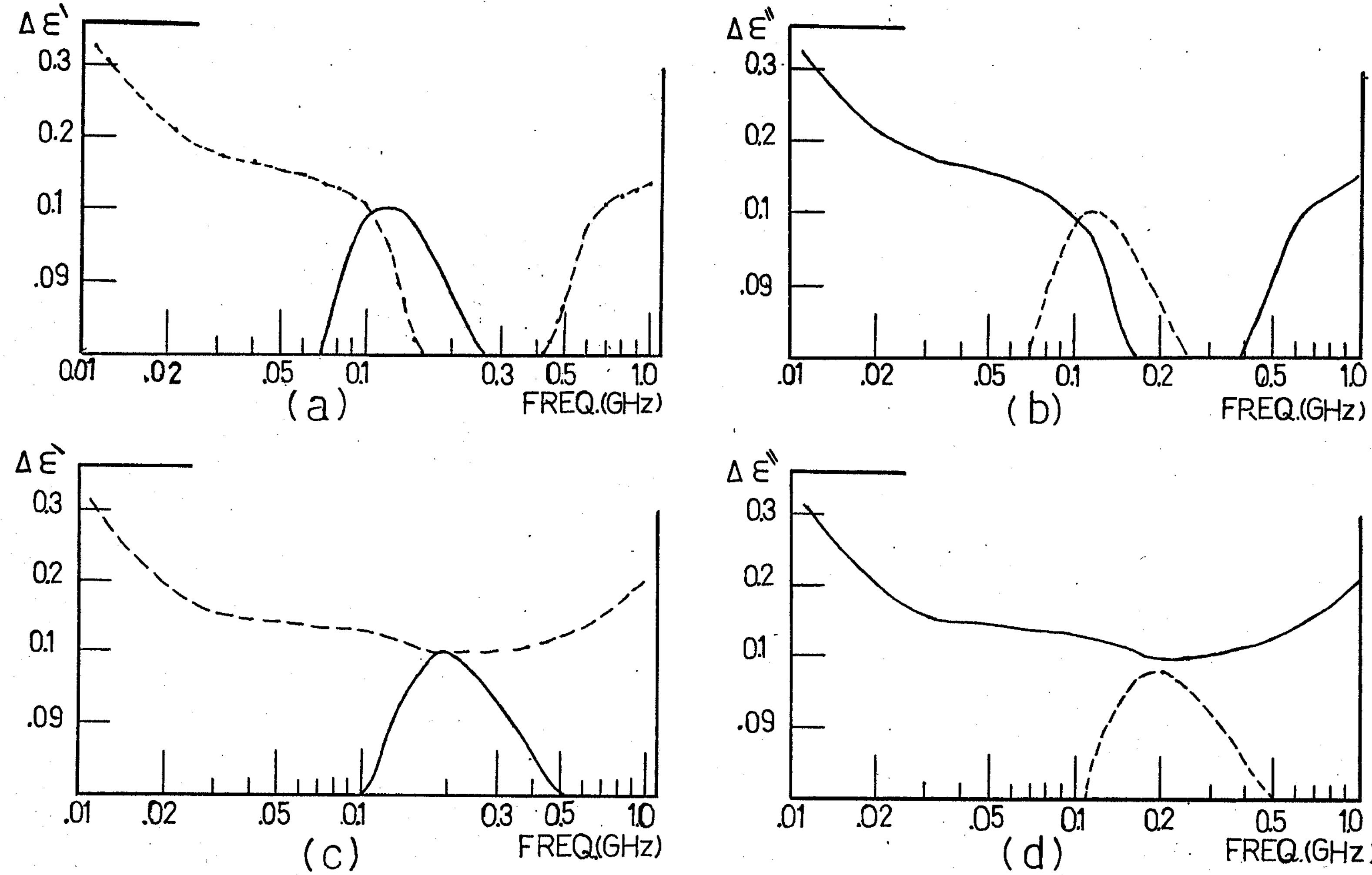

——— The uncertainties due to $\Delta |P|$

- - - - The uncertainties due to $\Delta \Theta$

Fig.10_ The uncertainties in ε' and ε'' due to the uncertainties in the modulus and phase of the reflection coeff.

a) and b) are for alkyl alcohol $C_8H_{17}OH$ at 16.5 C°

c) and d) are for alkyl alcohol $C_8H_{17}OH$ at 25 C°

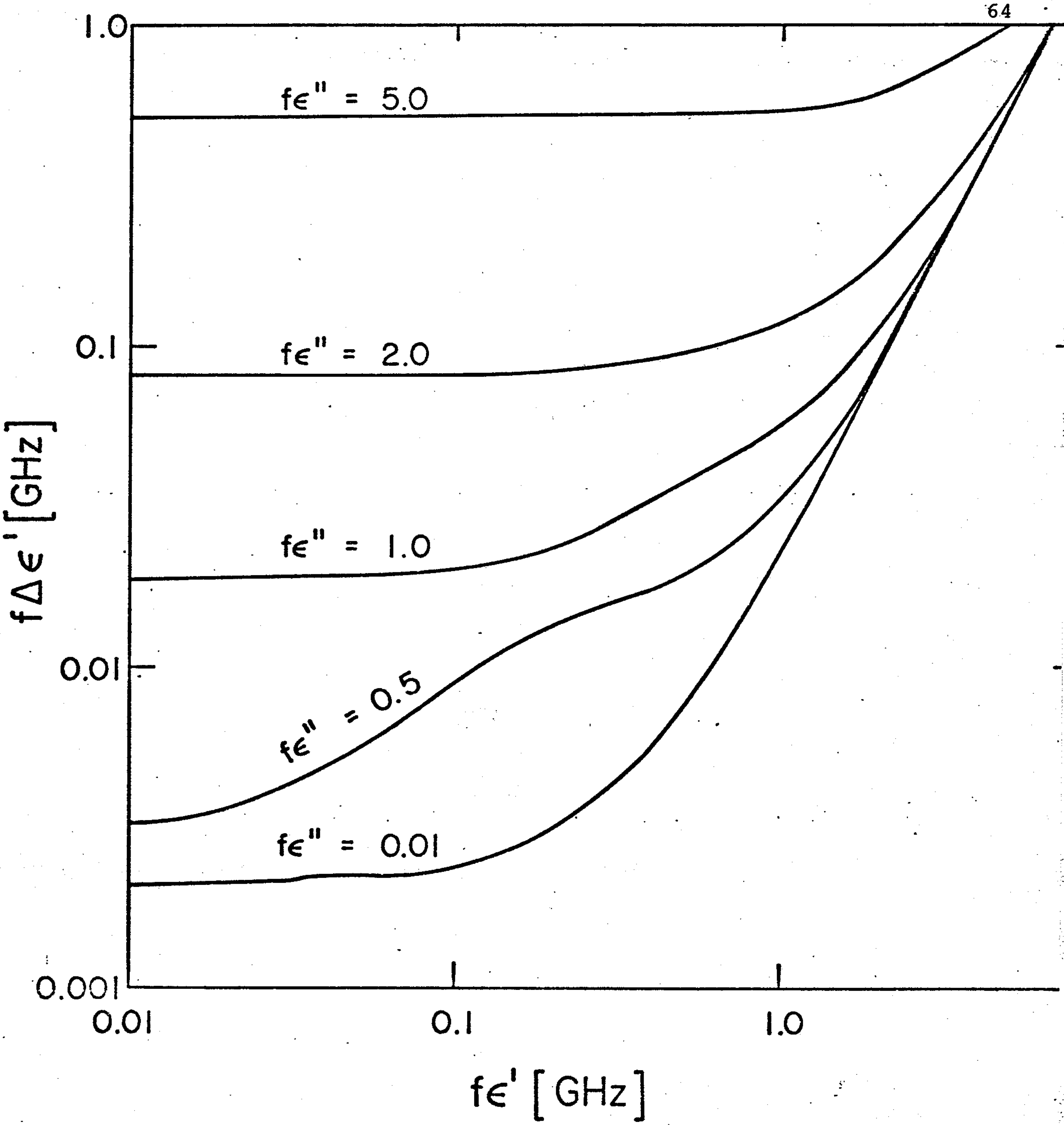

Fig.11. Uncertainty in measurement of $f\epsilon'$ as a function of $f\epsilon'$ for different values of $f\epsilon''$.

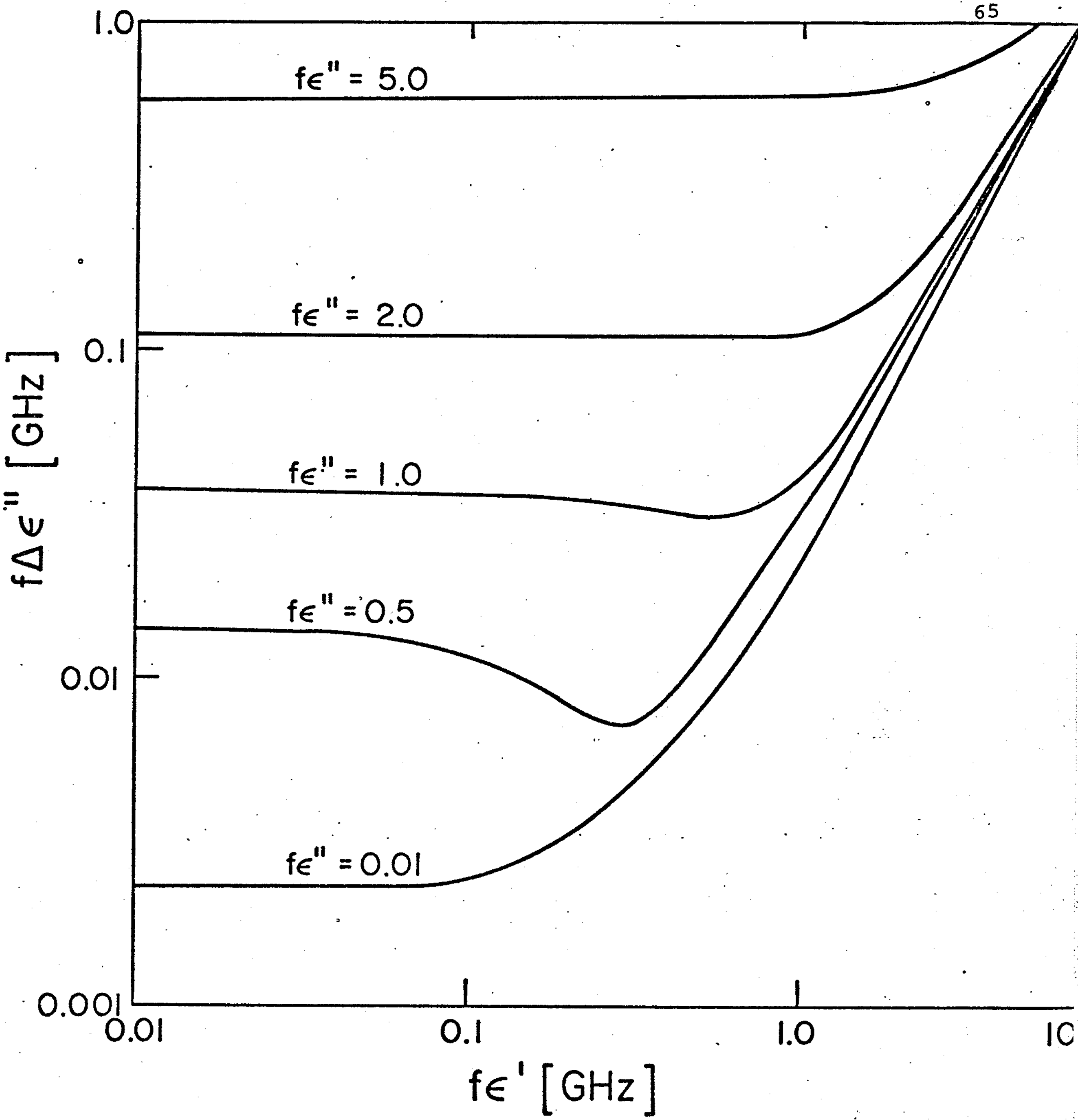

Fig.12. Uncertainty in measurement of $f\epsilon''$ as a function of $f\epsilon'$ for different values of $f\epsilon''$.

of the test capacitor $C_o = 10$ pf, and the characteristic impedance of the transmission line $Z_o = 50\ \Omega$. The following uncertainties were assumed: $\Delta C_o = 5 \times 10^{-14}$F, $\Delta Z_o = 0.1\ \Omega$ with $\Delta\rho = 1.4\%$ and $\Delta\theta = 0.8°$ in the frequency band from 0.01 to 1.0 GHz. A detailed analysis of the uncertainties shows that the most sensitive term is the uncertainty in the air capacitance of the test capacitor. Fortunately, this parameter can be determined with sufficient accuracy (less than 1% error) to damp the resulting uncertainty. The major contribution comes from the uncertainties in the modulus and phase angle of the reflection coefficient (Fig. 10).

Further analysis of Eqn. (26) and Eqn. (27) shows that the major frequency band limitation of the time domain method is related to the capacitance of the air-filled capacitor. Large capacitors give smaller uncertainties at lower frequencies and vice versa, small capacitances are better at higher frequencies. A compromise is usually required for any given frequency band. Additional high frequency limitation of this technique is due to the noise of the measuring system which becomes especially pronounced at higher frequencies as a result of the limited spectral intensity of the incident step.

5.3 Optimum value of the capacitance in a given frequency band

The direct relation between the frequency-band limitation and the capacitance of the air capacitor, suggested a technique to choose the optimum value of the capacitance for a specified frequency band, given some *a priori* knowledge of the dielectric properties of the sample under test. If the real and the imaginary parts of the complex permittivity (ε' and ε'') are required to be known within a certain preset tolerance in a specified frequency band, the optimum value of the capacitor can be calculated by a computer program which requires as inputs:

(1) the frequencies at the boundaries of the specified frequency band,

(2) the nominal values of ε' and ε'' at these frequencies,

(3) the allowed tolerances at these frequencies,

(4) the assumed values for the uncertainties ΔZ_o, ΔC_o, $\Delta|\rho|$ and $\Delta\theta$,

(5) the initial, final and incremental values of the capacitances, which is a running parameter in these calculations.

The optimum capacitance can be obtained by running the program to perform the following calculations:

(i) at the first specified frequency and for the initial values of the capacitance the uncertainties in ε' and ε'' are calculated and are denoted by $\Delta\varepsilon'$ and $\Delta\varepsilon''$.

(ii) The ratios of the specified tolerances ($\delta\varepsilon'$ and $\delta\varepsilon''$) to the calculated values are obtained. If the ratios

$$\frac{\delta\varepsilon'}{\Delta\varepsilon'} \leq 1 \quad \text{and} \quad \frac{\delta\varepsilon''}{\Delta\varepsilon''} \leq 1$$

then the calculated uncertainties are within the specified tolerances for this value of the capacitance.

(iii) The same procedure is repeated for all other values of the capacitances in the specified (capacitance) range.

(iv) We repeat exactly the same argument at the second specified frequency. We call

$$X = \frac{\delta\varepsilon'}{\Delta\varepsilon'} \quad \text{and} \quad Y = \frac{\delta\varepsilon''}{\Delta\varepsilon''}$$

The locus of X-Y as a function of capacitance is now plotted on the X-Y plane for the two specified frequencies.

(v) The values of the capacitances repeated in the acceptable region ($X \geq 1$ and $Y \geq 1$) on both curves are the acceptable values of the capacitances to be used in the specified frequency band with uncertainties $\leq$ the allowed tolerances.

The procedure will be illustrated by the following examples. The first example of the use of this technique to optimize the value of the capacitance is shown in

Fig. 13 for a dielectric material with $\varepsilon^* = 3.4 - j1.0$ (organic liquid-Aromatic-Arodor 1232) [2]. Setting the tolerance limit at $\delta\varepsilon' = \pm\ 0.5$ and $\delta\varepsilon'' = \pm\ 0.25$, we see that a capacitor of 9 pf capacitance can be used while the calculated uncertainties are less than the specified tolerance limits in the frequency band from 0.01 GHz to 1 GHz. It is also seen that the major limitation is due to the uncertainties in ε''.

For the same dielectric material Fig. 14 shows curves for tolerance limits at $\delta\varepsilon' = \pm\ 0.5$ and $\delta\varepsilon'' = \pm\ 0.3$. From these curves we see that there is more than one value for the capacitance to satisfy the specified requirements. Capacitors of capacitance varying from 8 pf to 11 pf can be used, but a capacitor of 8.8 pf will be the best to satisfy the specified tolerance limit in the frequency band of interest, from 0.01 GHz to 1 GHz. Figure 15 shows similar curves for dielectric material with $\varepsilon^* = 16.0 - j5.0$ and tolerance limits of $\delta\varepsilon' = 1.5$ and $\delta\varepsilon'' = 1.2$, which are quite large uncertainties. A capacitor of capacitance 2 pf can hardly satisfy the specifications. It is interesting to note that, for the dielectrics with high dielectric constant, the low frequency uncertainties are quite small (compared with the tolerance limit) and can easily be achieved by any capacitor of capacitance larger than 1.0 pf, while the high frequency accuracies are very difficult to achieve and require a capacitor of very small

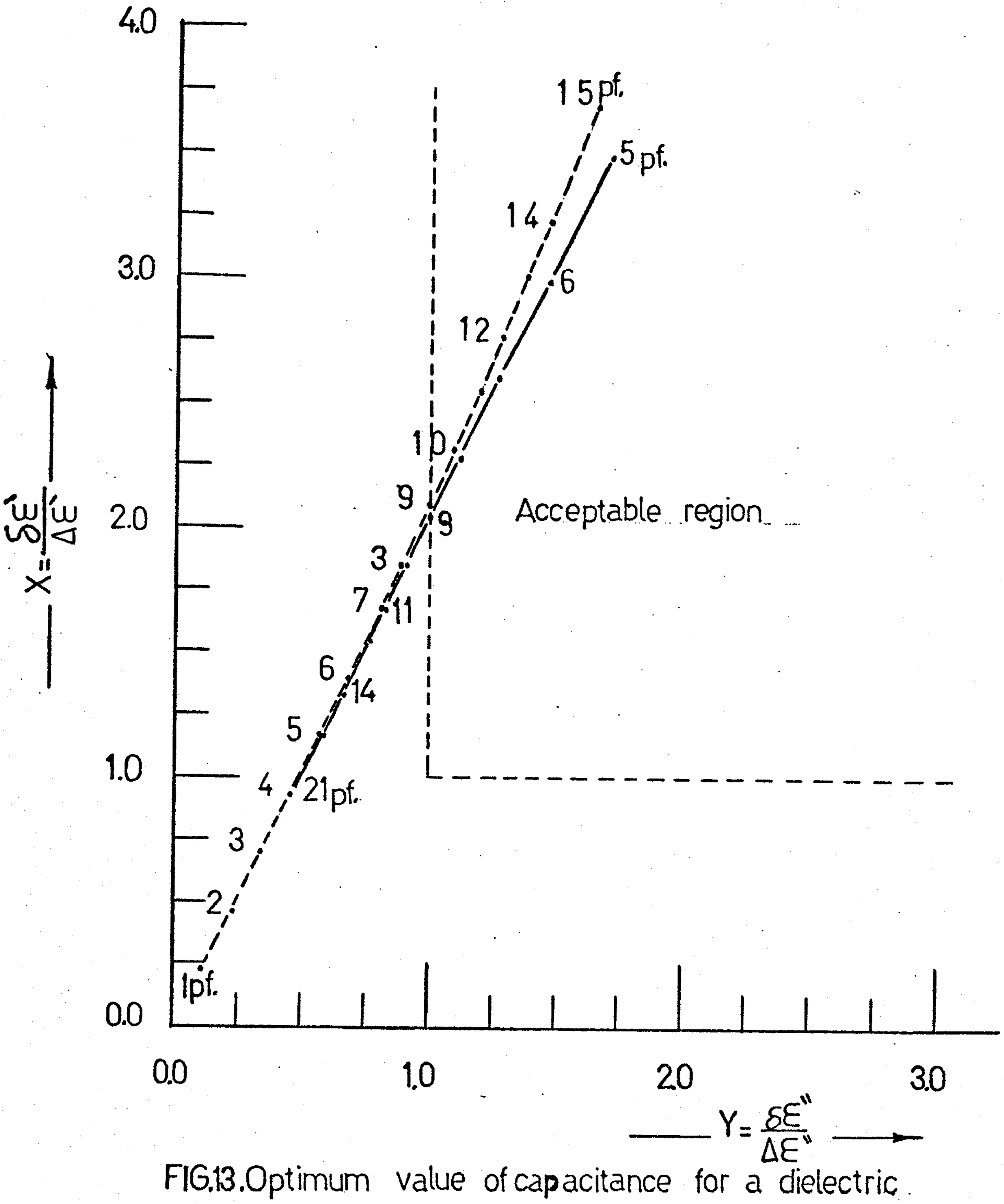

FIG.13. Optimum value of capacitance for a dielectric with $\epsilon^* = 3.4 - j1.0$. ($\delta\epsilon' = \pm 0.5$ and $\delta\epsilon'' = \pm 0.25$)

----- X.Y plot at 10 MHz.

——— X.Y plot at 1 GHz.

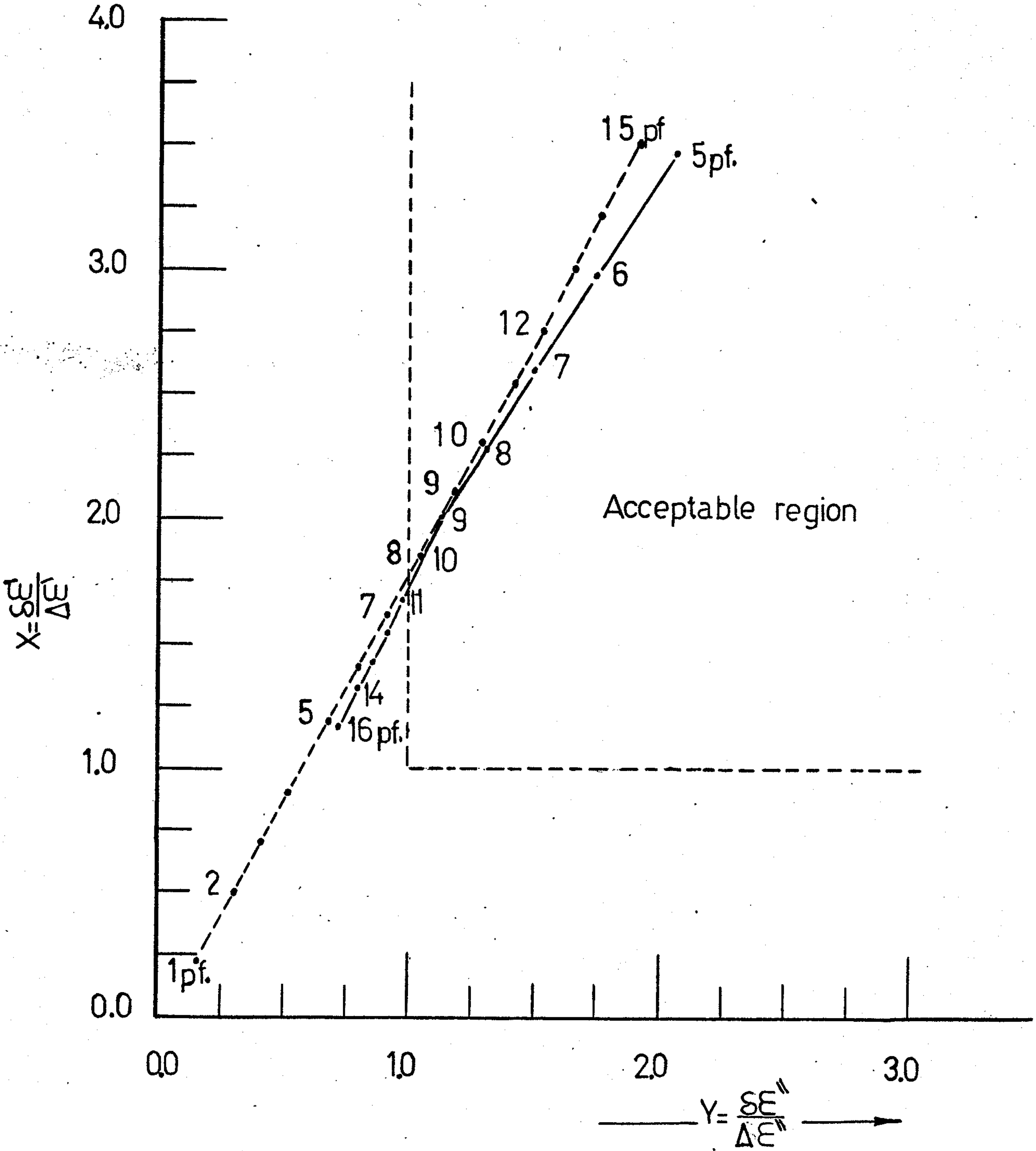

FIG.14. Optimum value of capacitance for a dielectric with $\varepsilon^* = 3.4 - j1.0$. ($\delta\epsilon' = \pm 0.5$ and $\delta\epsilon'' = \pm 0.3$)

---- X.Y plot at 10 MHz.

—— X.Y plot at 1 GHz .

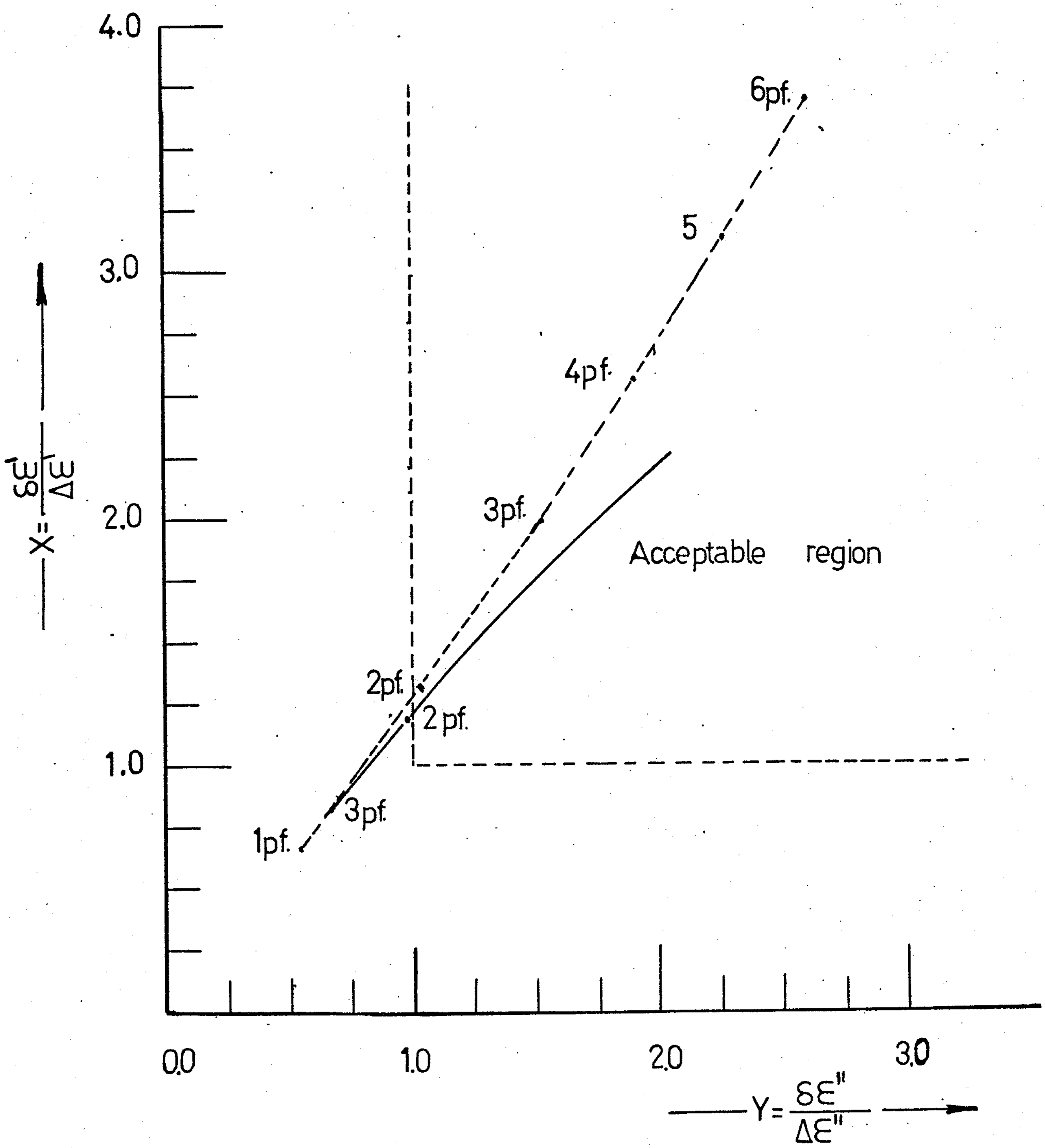

Fig.15. Optimum value of capacitance for a dielectric with $\varepsilon^* = 16.0 - j5.0$. ($\delta\varepsilon' = \pm 1.5$ and $\delta\varepsilon'' = \pm 1.2$).

\- - - - X.Y plot at 10 MHz.

_____ X.Y plot at 1 GHz.

capacitance (smaller than 2 pf). Figures 16 through 18 show the effect of the specified frequency-band[†] on the optimum value of the capacitance for the same dielectric and the same specified tolerance limits. A hypothetical dielectric of $\varepsilon^* = 5.0 - j1.0$ is used as a demonstrative example, with specified tolerances of $\pm$ 0.5 in both ε' and ε''. It is interesting to note that for high frequency applications, smaller capacitances are required and conversely larger capacitances are required for low frequency measurements.

[†] This is done under the assumption that the specified figures of the uncertainties in $\Delta|\rho|$ and $\Delta\theta$ still holds for the frequency band from 0.05 GHz to 2 GHz.

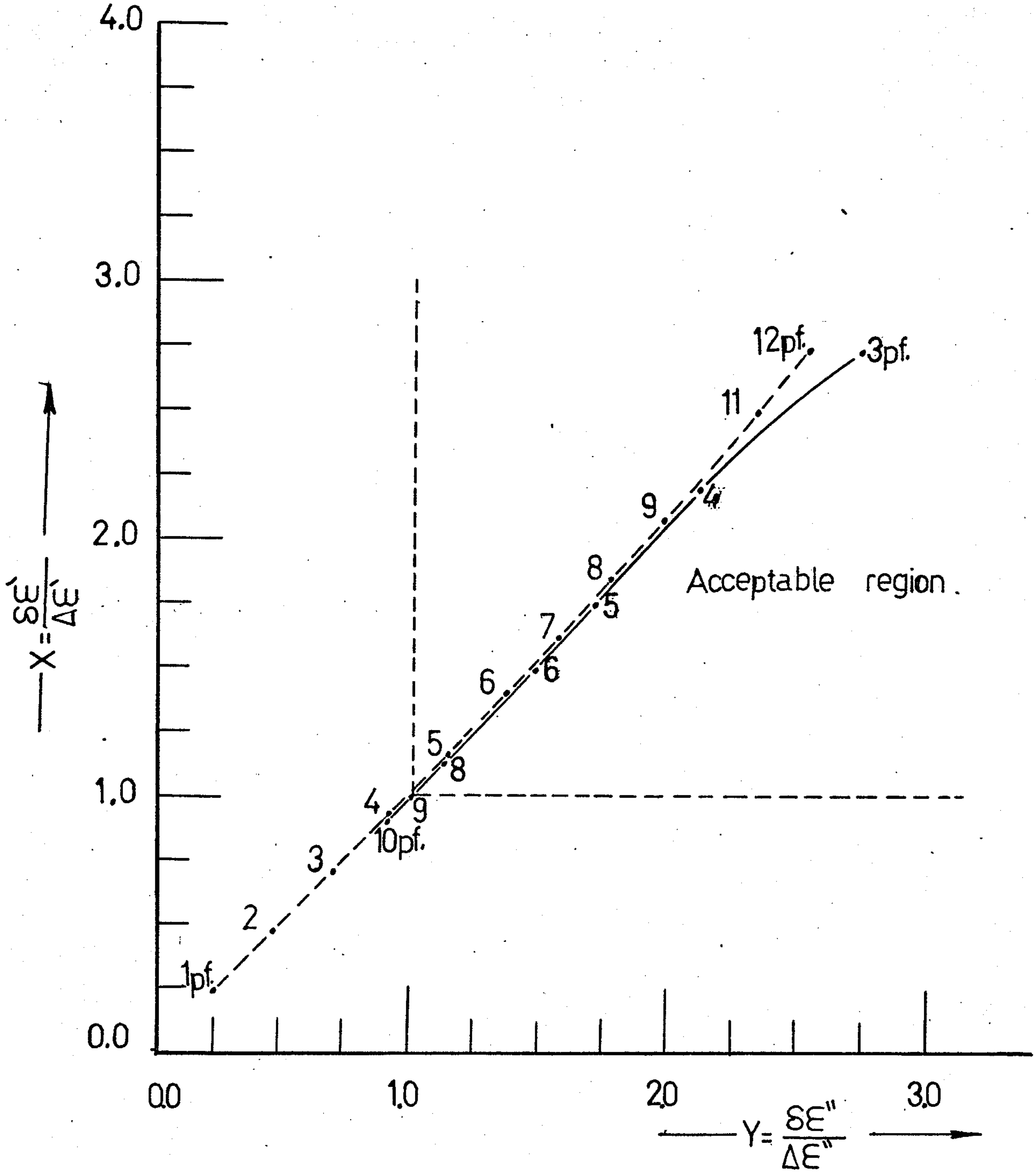

Fig.16. Optimum value of capacitance for a dielectric with $\epsilon^* = 5.0 - j1.0$. ($\delta\epsilon' = \pm 0.5$ and $\delta\epsilon'' = \pm 0.5$).

---- X.Y plot at 10 MHz.

____ X.Y plot at 1GHz .

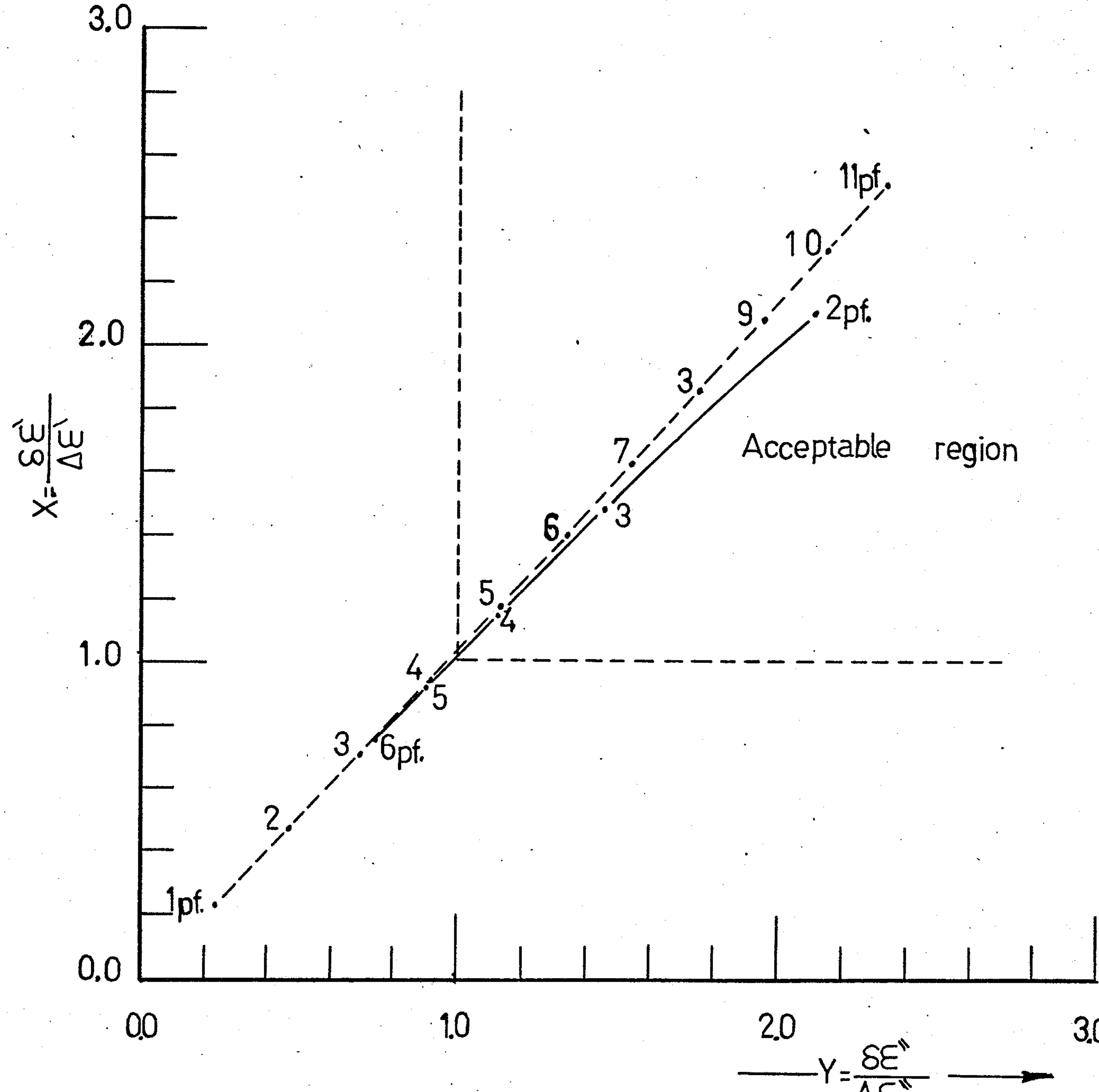

Fig.17 Optimum value of capacitance for a dielectric with $\varepsilon^* = 5.0 - j1.0$. ($\delta\epsilon' = \pm 0.5$ and $\delta\epsilon'' = \pm 0.5$).

---- X-Y plot at 10MHz,

_____ X-Y plot at 2GHz.

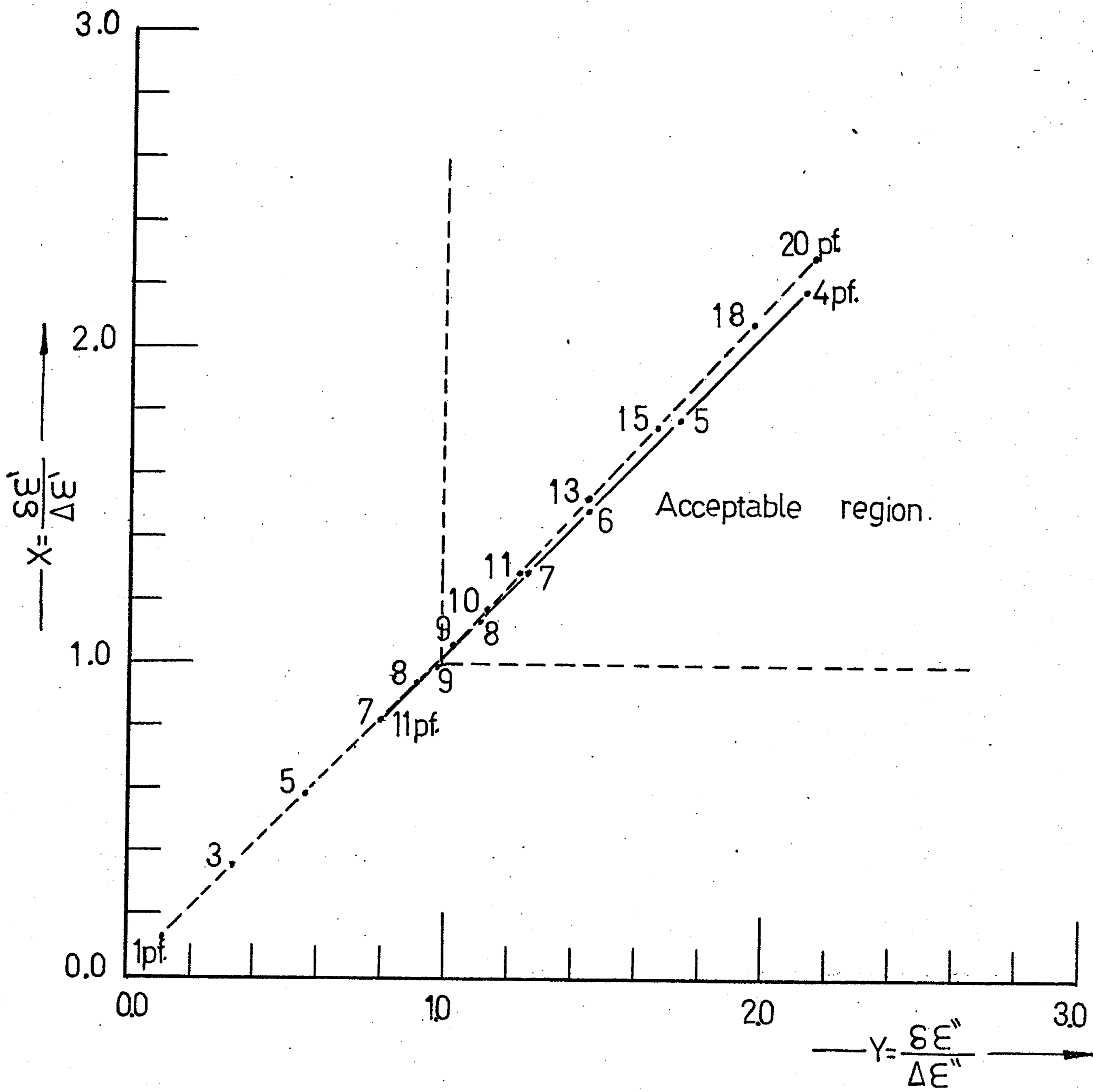

Fig.18. Optimum value of capacitance for a dielectric with $\varepsilon^* = 5.0 - j1.0$. ($\delta\varepsilon' = \pm 0.5$ and $\delta\varepsilon'' = \pm 0.5$).

---- X.Y plot at 5MHz.

—— XY plot at 1GHz.

CHAPTER 6

MEASUREMENT TECHNIQUE AND EXPERIMENTAL RESULTS

In this chapter, the measurement technique to determine experimentally the frequency spectrum of the reflection coefficient is described. Experimental results are presented and compared with available data in the literature.

6.1 Measurement technique

In order to determine experimentally the frequency dependence of the reflection coefficient $\rho(\omega)$, the following measurement procedure has been adopted.

When the sample holder is short-circuited at the plane A-A in Fig. 4(a) the wave form displayed by the oscilloscope is $V_{sc}(t-t_o)$ where

$$t_o = \frac{\text{distance between the sampler and A-A}}{\text{speed of light}}$$

For a perfect short circuit, $V_{sc}(t-t_o) = -V_{in}(t-t_o)$ where V_{in} is the incident wave. With the test sample between the plates of the capacitor the displayed waveform will be

$$V_o(t) = V_{in}(t-2t_o) + V_r(t-t_o)$$

and

$$V_o(t) - V_{in}(t-2t_o) = V_r(t-t_o)$$
$$= V_{in}(t-t_o) * \rho(t)$$

where V_r is the reflected wave, $\rho(t)$ is the time response of the reflection coefficient and $*$ denotes a convolution. Finally, both displayed waveforms V_{sc} and V_o are digitized and a discrete Fourier transform is calculated using a digital computer with the necessary corrections in order to eliminate a large truncation error in step-like functions [11]. The reflection coefficient is then calculated by taking the ratio of both discrete Fourier transforms, i.e.,

$$\rho(\omega) = |\rho(\omega)|e^{-j\theta(\omega)}$$

$$= \frac{FV_r(t-t_o)}{FV_{in}(t-t_o)}$$

$$= \frac{F[V_{in}(t-t_o) * \rho(t)]}{FV_{in}(t-t_o)}$$

$$= \frac{F[V_o(t) - V_{in}(t-2t_o)]}{-FV_{sc}(t-t_o)}$$

The frequency spectrum of the real and imaginary parts of the relative permittivity is thus found from Eqn. (14) and Eqn. (15).

6.2 Experimental results

Feasibility of the method was evaluated experimentally by measurements of the dielectric properties of some polar liquids and some substances which have very short relaxation times like teflon and mica.

The size of the sample was basically determined by the dimensions of the gap between the inner conductor of the sample holder and the terminating metal plate, as well as by the viscosity of the liquid in the case of liquid samples. In the reported experiments the sample holder was kept in the vertical position in order to avoid spilling of the liquid samples, although any liquid film present on the terminating plate has negligible effect on the system response due to the fact that the electric field at this surface is also negligibly small.

The experimental results in Fig. 19 through Fig. 21 are generally in good agreement with the data obtained by the frequency domain methods in [21] and [22]. Large differences are observed between our experimental results and the values of ε' and ε'' calculated from the data in [12] (represented by triangles). This is probably due to the incorrect relaxation times given in [12] as suggested in [13].

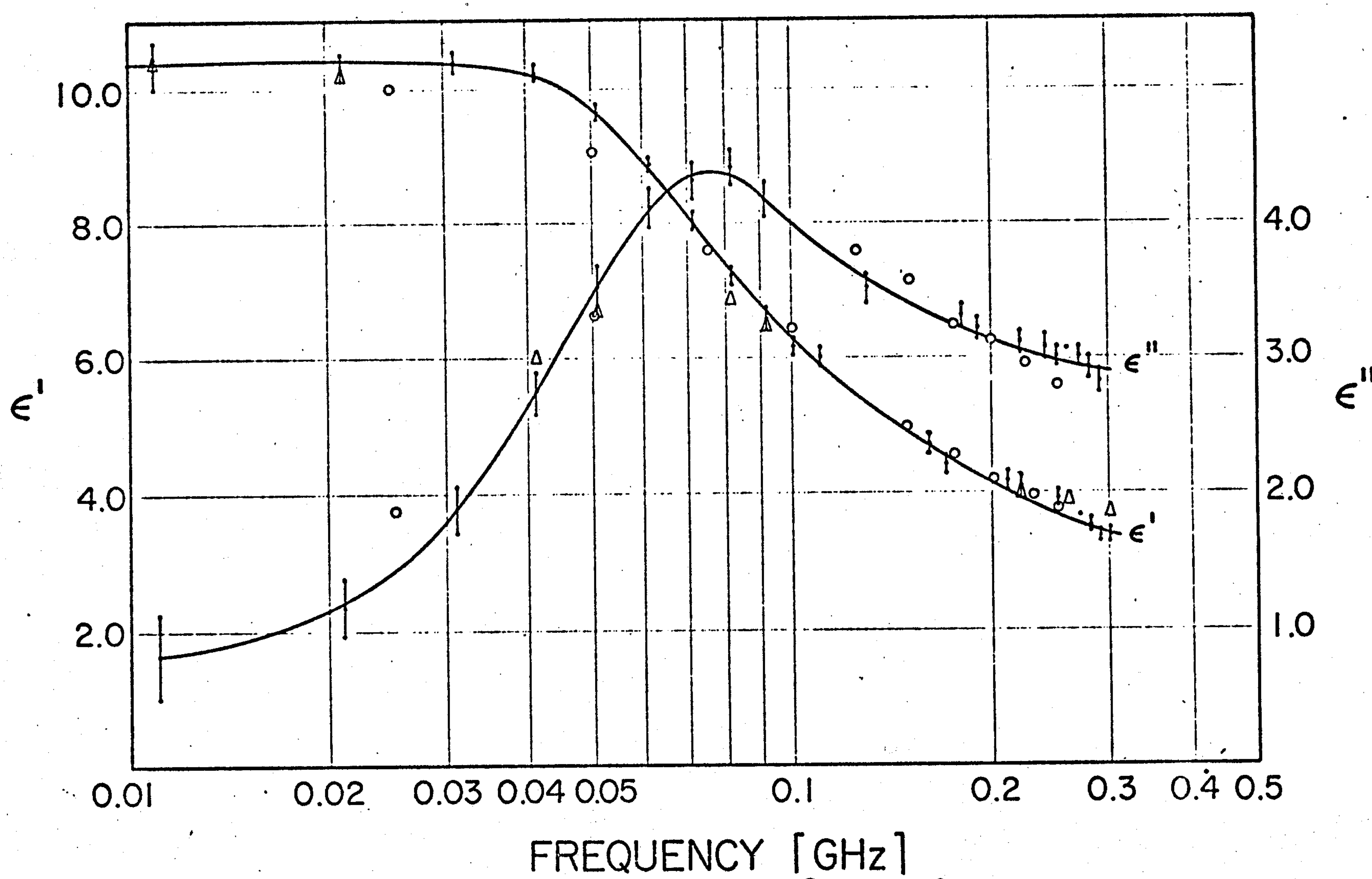

Fig.19. Experimental results for the alkyl alcohol, $C_8H_{17}OH$ at 16.5°C.
Δ - points calculated based on data given in [12] assuming the ideal Debye dispersion with a single relaxation time.
o - experimental points from [21].

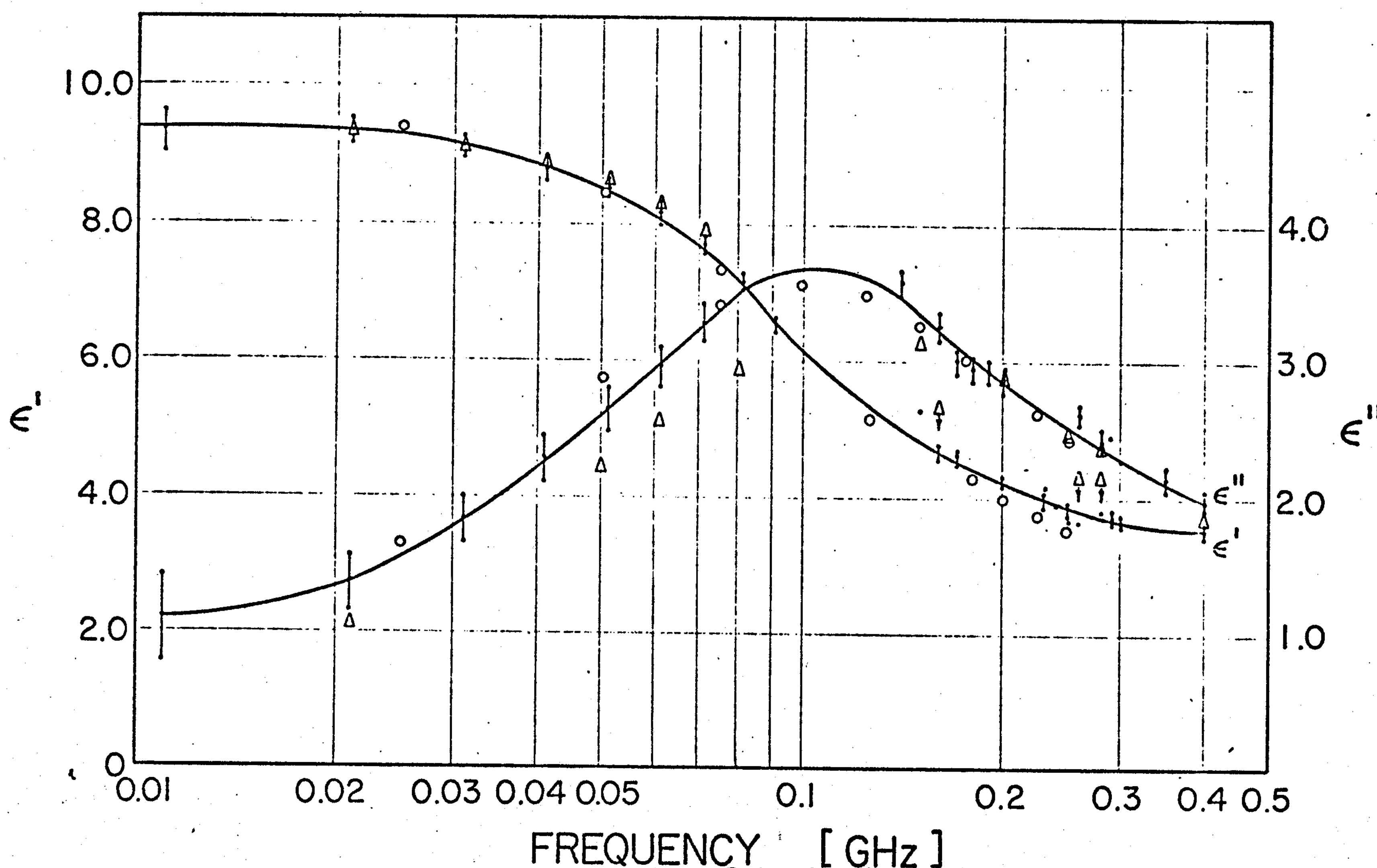

Fig.20 Experimental results for the alkyl alcohol $C_8H_{17}OH$ at 25°C.

Δ – points calculated based on data given in [12] assuming the ideal Debye dispersion with a single relaxation time. o – experimental points from [21].

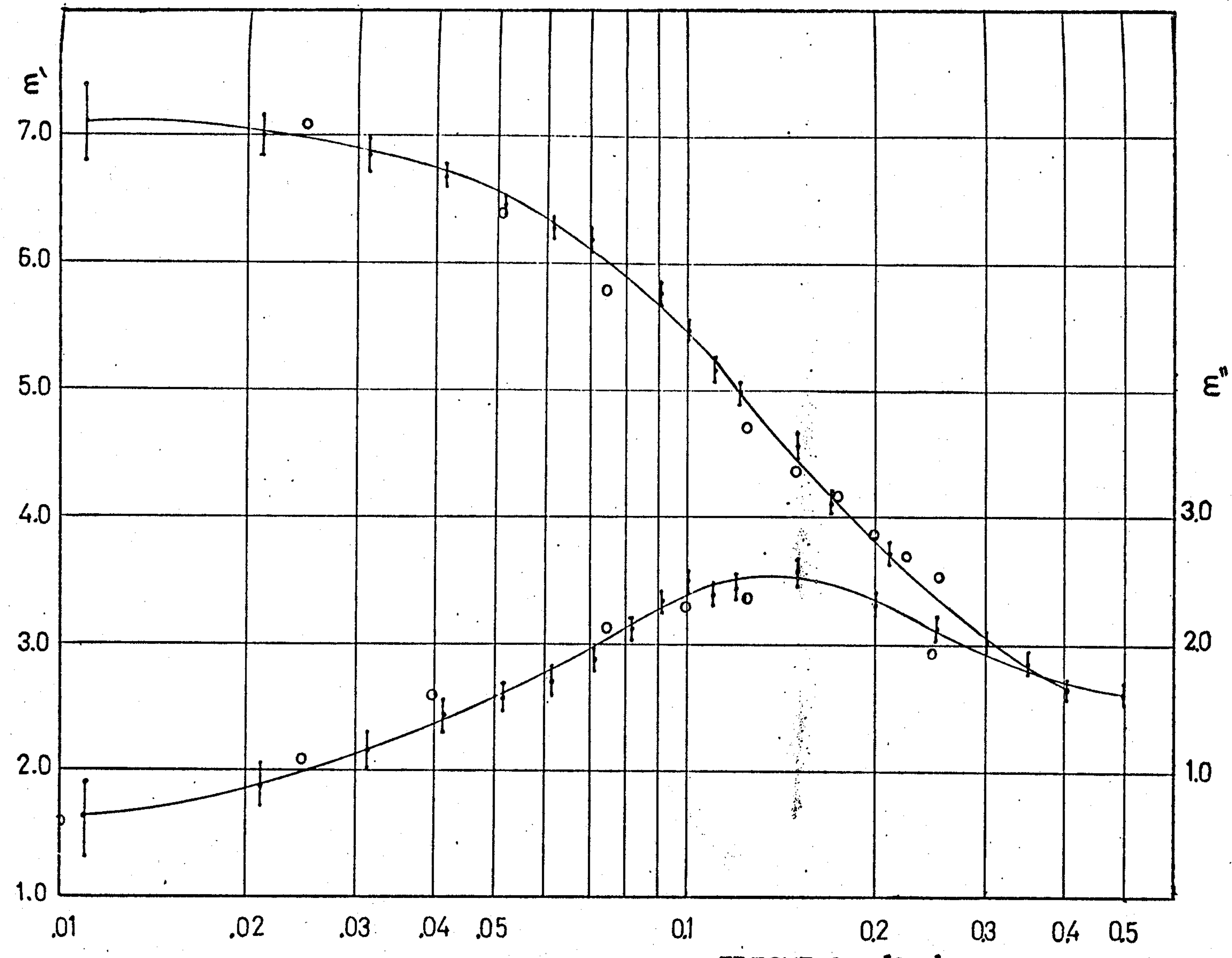

Fig.21 Experimental results for alkyl alcohol $C_{10}H_{21}OH$ at 25°C. o_experimental points from [21].

The experimental results for dielectric sheets of teflon and mica in Fig. 22 and Fig. 23 are in good agreement with the data in [2]. Vertical lines show the estimated uncertainties.

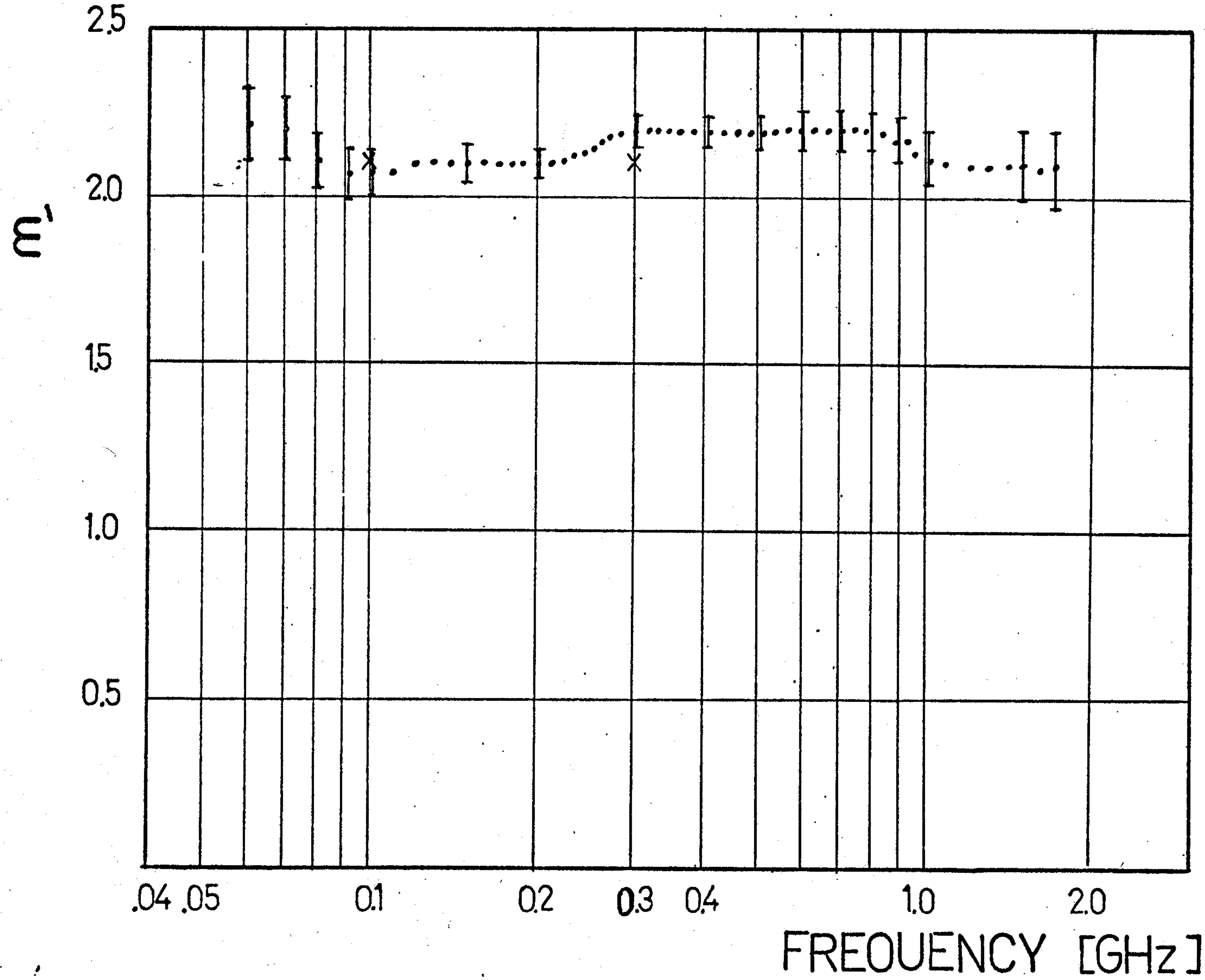

Fig.22. Experimental results for Teflon sheet at 25°C.
x– experimental points from [2]

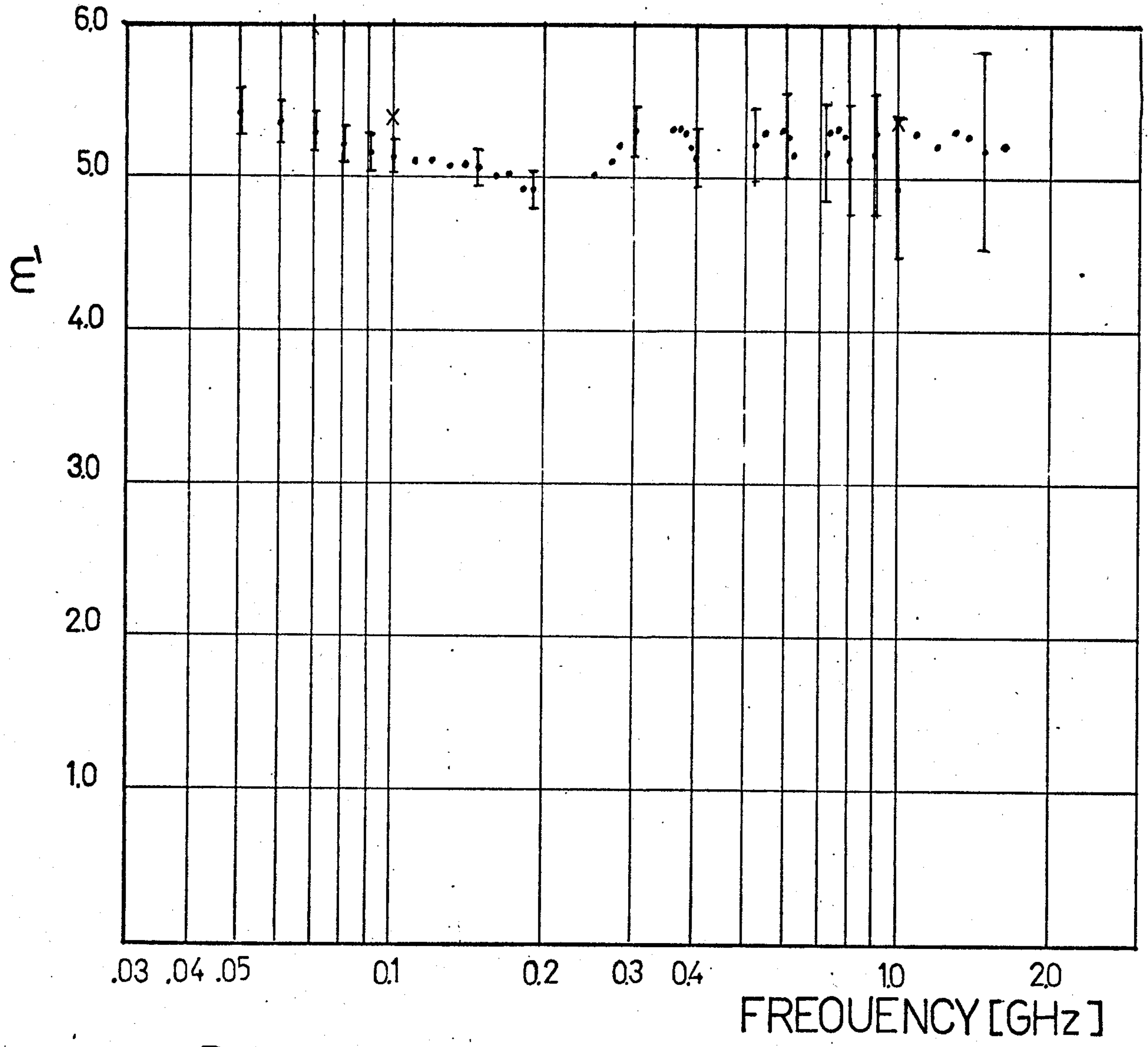

Fig.23. Experimental results for Mica sheet at 25°C.
x_ experimental points from [2]

CHAPTER 7

CONCLUSIONS

A novel technique for permittivity measurements in time domain, which utilizes a small shunt capacitor terminating a coaxial line section as a sample holder, has been described. This technique gives all necessary information on the frequency behaviour of the tested substance, while the required sample volume is of the order of a cubic millimeter.

Theoretical analysis of the time dependence of the reflection coefficient following application of a step voltage to a shunt capacitor located at the end of a transmission line and filled with the dielectric under test has been derived for some dispersion mechanisms of potential interest in biological studies.

Analysis and calculations of the overall uncertainty of permittivity measurements are given. This analysis shows that the major frequency band limitation is related to the air capacitance of the test capacitor. Large capacitancies give smaller uncertainties at lower frequencies and conversely small capacitances are better at higher frequencies. A compromise is usually required for any given frequency band and dielectric.

The direct relation between the frequency band limitation and the value of the air capacitance suggested a technique to choose the optimum value of the test capacitor for a specified frequency band. This technique was presented with several illustrative examples.

Feasibility of the proposed method was evaluated experimentally by measurements of the dielectric properties of some polar liquids and some substances which have very short relaxation times like teflon and mica. Generally good agreement was achieved with the data available from point by point frequency domain methods.

The greatest assets of this technique are its speed, simplicity, relative ease of data evaluation and a very small sample required.

This work has laid the basis for further time domain studies to improve the system for more accurate measurements in a wider frequency band. This will require the development of higher-voltage generators, the synthesis of waveforms with more spectral energy at higher frequencies and the adoption of more efficient signal processing techniques.

REFERENCES

1. Smyth, C.P., "Dielectric Constant and Molecular Structure", The Chemical Catalog Company, New York (1931).

2. Von Hippel, A., "Dielectric Materials and Applications", MIT Press, Cambridge, Mass. (1954).

3. Anderson, J.C., "Dielectrics", Chapman and Hall Ltd., London (1963).

4. Hill, N.E., Vaughan, W.E., Price, A.H. and Divides, M., "Dielectric Properties and Molecular Behaviour", Van Nostrand Reinhold Company, London (1969).

5. Schwan, H.P., "Determination of biological impedances", Physical Techniques in Biological Research, Vol. VI, Chapter 6, Academic Press (1963).

6. Schwan, H.P., "Electrical properties of tissue and cell suspensions", Advan. Biol. Med. Phys., Vol. 5, pp. 147-209 (1957).

7. Schwan, H.P., "Application of VHF impedance measuring techniques in biophysics", IRE Transaction on Instrumentation, pp. 75-83, Oct. (1955).

8. Conference on precision electromagnetic measurements, Session IIIB, Boulder,Colorado, June (1972).

9. Almassy, G., Misik, M.B.S., "Determination of the properties of the bound water in biological object by microwave methods", presented in CPEM, Boulder, Colorado, 1972.

10. Nicolson, A.M., Ross, G.F., "Measurement of the intrinsic properties by time-domain technique", IEEE Trans. Instrum. Meas., Vol. IM-19, No. 4, pp. 377-382, November (1970).

11. Ross, G.F., Nicolson, A.M., Smith, R., Susman, L., Hanley, G., "Transient behaviour of microwave networks", Sperry Rand Research Center, Report No. SRRR-CR-68-2 (1968).

12. Fellner-Fedlegg, H., "The measurement of dielectrics in the time-domain", Jour. Phys. Chem., Vol. 73, No. 3, pp. 616-623, March (1969).

13. Fellner-Fedlegg, H., Barnett, E.F., "Reflection of a voltage step from a section of transmission line filled with a polar dielectric", Jour. Phys. Chem., Vol. 74, No. 9, pp. 1962-1965, April (1970).

14. Nicolson, A.M., Bennett, C.L., Lamensdors, D., Susman, L. "Applications of time domain metrology to the automation of broad-band microwave measurements", IEEE Transaction, Vol. MTT-20, No. 1, January (1972)

15. Frohlich, H., "Theory of Dielectrics", Oxford Univ. Press, London (1958),p. 98.

16. Papoulis, A., "The Fourier Transform and Its Application", McGraw-Hill, New York, (1962),p. 48.

17. Hewlett-Packard Appl. Note 118 (1970).

18. Green, H.E., "The numerical solution of some important transmission line problems", IEEE Trans. Mic. Theory and Tech., Vol. MTT-13, pp. 677-692 September (1965).

19. Kline, S.J., McClintock, F.A., "Describing uncertainties in single-sample experiments", Mech. Eng., p. 3, January (1953).

20. Marcuvitz, N., "Waveguide Handbook" First Edition, McGraw-Hill, New York, Sect. 5, Chapter 4, p. 178 (1951).

21. Denney, D.J., Cole, R.H., Jour. Chem. Phys., Vol. 25, p. 1767 (1955).

22. Garg, S.K., Smyth, C.P., "Microwave absorption and molecular structure in liquids.LXII. The three dielectric dispersion regions of the normal primary alcohols", Jour. Phys. Chem. Vol. 69, No. 4, pp. 1294-1301 (1965).

APPENDIX 1

TIME JITTER STANDARD DEVIATION [11]

The standard deviation σ_τ of the triggering time jitter was found by stopping the scan at a position on a waveform where the slope was large and taking several hundred samples. The variance of these samples was much greater than the noise variance. From a subsequent slow scan across this part of the waveform the slope could be determined, and from this slope and the voltage variance due to jitter, the time variance could be found.

e.g. At a point on the waveform where the slope was 18.1 volt/n sec, the voltage SD due to noise and jitter was 35 mV. Thus, the SD due to jitter was

$$\sqrt{(35)^2 - (6)^2} = 34.5 \text{ mV}$$

where 6 substitutes the SD of the noise voltage

time jitter SD $\sigma_\tau = \dfrac{34.5}{18.1} = 1.9$ n sec.

APPENDIX 2

COMPUTER PROGRAMS

Time to frequency domain programs

The following are two computer programs written in FORTRAN IV. The first one evaluates the continuous Fourier transform, writing the real and imaginary parts at the particular required frequencies. The input parameter KIND is normally zero; when set to -1, the step correction is applied.

The second one uses the Fourier transform of both the input step and the reflected wave to form the frequency spectrum of the reflection coefficient. The values of ε' and ε'' are then calculated using Eqns. (14) and (15).

```
C     CONTINUOUS  FOURIER  TRANSFORM
      DIMENSION A(900)
      MM=0
      READ50,LL
    5 IF(MM-LL)10,1000,1000
   10 PI=3.141592654
      P2=PI+PI
      PO2=PI/2.
      FAC=180./PI
      READ100,N,KIND
      DO 20 I=1,N
      READ200,A(I)
   20 PRINT300,A(I)
      READ400,DELTAT,FSTART,DELTAF,NFREQ
      IMAX=NFREQ+1
      Z=P2*DELTAT
      B=FSTART
      PRINT500
      DO13 I=1,IMAX
      WH=B*Z
      R=0.0
      S=0.0
      T=0.0
      DO14 L=1,N
      R=R+A(L)*COS(T)
      S=S-A(L)*SIN(T)
      T=T+WH
   14 CONTINUE
      IF(KIND)38,39,39
   38 IF(WH-1.E-6)39,40,40
   40 X=A(N)/(2.*SIN(WH/2.))
      Y=(WH*(N-.5))+PO2
      R=R+(X*COS(Y))
      S=S-(X*SIN(Y))
   39 C=DELTAT*SQRT((R*R)+(S*S))
      PRINT600,R,S
      PUNCH600,R,S
      THETA=FAC*ATAN(S/R)
      PRINT700,B,C,THETA
      B=B+DELTAF
   13 CONTINUE
      MM=MM+1
      GO TO 5
   50 FORMAT(I4)
  100 FORMAT(2I4)
  200 FORMAT(F7.4)
  300 FORMAT(10X,F7.4)
  400 FORMAT(3F10.5,I4)
  500 FORMAT(10X,37HFREQ(GHZ)     AMPLITUDE      TRUE PHASE)
  600 FORMAT(10X,2E15.7)
  700 FORMAT(10XF7.3,4X,F9.5,5X,F9.3)
 1000 STOP
      END
```

```
$JOB    WATFIV
C    REFLECTION   COEFFICIENT
         DIMENSION C(2,300),D(2,300),B(300),DELTAT(2)
     101 READ100,N,FSTART,DELTAF
         READ800,Z0,C0
         READ 900,E0,E00,AT
         DO 1 IDO=1,2
         I0=-1
         I1=-1
         B0=-.002
         B1=-.001
         IND=-1
         READ200,(C(IDO,IJ),D(IDO,IJ),IJ=1,N)
         READ250,DELTAT(IDO)
         DO 13 I=1,N
         R=C(IDO,I)
         S=D(IDO,I)
         C(IDO,I)=SQRT((R*R)+(S*S))
         THETA=ATAN(S/R)
         C(IDO,I)=DELTAT(IDO)*C(IDO,I)
         IF(R)16,15,15
      15 I2=1
         GO TO 17
      16 I2=-1
      17 IF(S)19,18,18
      18 I2=I2+2
         GOTO81
      19 I2=I2-2
      81 IF(I2-3)21,20,21
      21 IF(I2-1)22,23,22
      22 IF(I2+3)24,23,24
      24 THETA=THETA+6.283185
         GOTO20
      23 THETA=THETA+3.14159265
      20 I3=4*I1-I2
         IF(I3-13)41,55,41
      41 IF(I3+15)42,70,42
      42 IF(I3+7)43,70,43
      43 IF(I3+5)45,70,45
      45 IF(I3-1)46,54,46
      46 IF(I3+1)49,54,49
      49 IF(I3+13)80,54,80
      55 IF(I0-I1)71,51,71
      51 IF(B0-B1)80,71,80
      54 IF(I0-I1)80,52,80
      52 IF(B1-B0)80,70,80
      70 IND=IND+1
         GO TO 80
      71 IND=IND-1
      80 THETA=THETA+6.283185*IND
         D(IDO,I)=THETA
         I0=I1
         I1=I2
         B0=B1
         B1=THETA
      13 CONTINUE
       1 CONTINUE
         DO 301 I=1,N
         B(I)=C(1,I)/C(2,I)
     301 CONTINUE
```

```
      PRINT600
      Z=FSTART
      DO 303 I=1,N
      X=B(I)
      Y=D(1,I)-D(2,I)
      A=COS(Y)
      R=SIN(Y)
      XX=(X*X)
      YY=(2.*X*A)
      H=(6.283185*Z*Z0*CC)
      HH=(XX+YY+1.)
      E1=-(2.*X*R)/(H*HH)
      E11=(1.-XX)/(H*HH)
      TE1=E00+((E0-E00))/(1.+(6.283185*Z*AT)**2.))
      TE11=((E0-E00)*6.283185*Z*AT)/(1.+(6.283185*Z*AT)**2.)
      PRINT700,Z,X,Y,E1,TE1,E11,TE11
      Z=Z+DELTAF
  303 CONTINUE
  100 FORMAT(I4,2F10.5)
  200 FORMAT(10X,2E15.7)
  250 FORMAT(F10.5)
  600 FORMAT(6X,'FREQ(GHZ)     AMP            PHASE-DIFF            E1
     2        TRUE-E1              E11             TRUE-E11')
  700 FORMAT(6X,F8.4,4X,F9.4,5X,F10.4,6X,F10.5,6X,F10.5,
     36X,F10.4,6X,F10.4)
  800 FORMAT(2E14.8)
  900 FORMAT(3(F7.4))
      GO TO 101
      END
```

<u>Uncertainty analysis programs</u>

The following are the programs used in the uncertainty analysis, as well as, the optimum value of the capacitance calculations. The first calculates the uncertainties in $f\varepsilon'$ and $f\varepsilon''$ as a function of $f\varepsilon'$ with $f\varepsilon''$ as a running parameter.

The second program computes the ratio of a given specified tolerance limit to the calculated uncertainties in ε' and ε'' with the value of the capacitance as a running parameter. This method was used to estimate the optimum value of capacitance to be used in a given frequency band given prior knowledge of the dielectric properties of the sample under test.

```
C     UNCERTAINTY ANALYSIS CALCULATIONS
    1 WRITE(6,10)
   10 FORMAT(40X,'UNCERTAINTY ANALYSIS CALCULATIONS')
      WRITE(6,11)
   11 FORMAT(20X,'FE11                          FE1                         FDE1
     2                    FDE11')
      READ(5,20)FFE1,EFE1,DFE1,FFE11,EFE11,DFE11
   20 FORMAT(6F10.4)
      READ(5,21)CO,ZO,DQ,DL,DCO,DZO
   21 FORMAT(E14.8)
      FE11=FFE11
    3 FE1=FFE1
   91 A=(CO*ZO*FE11*6.2831853)
      B=(CO*ZO*FE1*6.2831853)
      C=((1.+A)*(1.+A))+(B*B)
      AL=(SQRT((((1.-(A*A))-(B*B))*((1.-(A*A))-(B*B)))
     3+(4.*B*B)))/C
      U=(2.*B)
      V=((1.-(A*A))-(B*B))
      Q=ATAN2(U,V)
      H=(((AL*COS(Q))+1.)**2.)+((AL*SIN(Q))*(AL*SIN(Q)))
      DE12=(2.*AL*SIN(Q))/(6.2831853*CO*CO*ZO*H*0.1E-08)
      DE13=(2.*AL*SIN(Q))/(6.2841853*CO*ZO*ZO*H)
      DE14=(2.*SIN(Q)*(1.-(AL*AL)))/(6.2831853*CO*ZO*H*H)
      DE15=((2.*AL*AL*AL*COS(Q))+(2.*AL*COS(Q))+(4.*AL*AL))
     4/(6.2831853*CO*ZO*H*H)
      F1=((DE12)*DCO)*((DE12)*DCO)
      F2=((DE13)*DZO)*((DE13)*DZO)
      F3=((DE14)*DL)*((DE14)*DL)
      F4=((DE15)*DQ)*((DE15)*DQ)
      FDE1=SQRT(F1+F2+F3+F4)
      DE22=(1.-(AL*AL))/(6.2831853*CO*CO*ZO*H*0.1E-08)
      DE23=(1.-(AL*AL))/(6.2831853*CO*ZO*ZO*H)
      DE24=((4.*AL)+((2.*COS(Q))*((AL*AL)+1.)))/(6.2831853*CO*ZO*H*H)
      DE25=((1.-(AL*AL))*2.*AL*SIN(Q))/(6.2831853*CO*ZO*H*H)
      Y1=((DE22)*DCO)*((DE22)*DCO)
      Y2=((DE23)*DZO)*((DE23)*DZO)
      Y3=((DE24)*DL)*((DE24)*DL)
      Y4=((DE25)*DQ)*((DE25)*DQ)
      FDE11=SQRT(Y1+Y2+Y3+Y4)
      WRITE(6,12)FE11,FE1,FDE1,FDE11
      TE1=FFE1*10.0
      IF(FE1-TE1)90,100,100
   90 FE1=FE1+DFE1
      GO TO91
  100 DFE111=DFE1
  105 DFE111=DFE111*10.0
      TE1=10.*TE1
  101 IF(TE1-EFE1)102,102,103
  102 FE1=FE1+DFE111
      A=(CO*ZO*FE11*6.2831853)
      B=(CO*ZO*FE1*6.2831853)
      C=((1.+A)*(1.+A))+(B*B)
      AL=(SQRT((((1.-(A*A))-(B*B))*((1.-(A*A))-(B*B)))
     3+(4.*B*B)))/C
      U=(2.*B)
      V=((1.-(A*A))-(B*B))
      Q=ATAN2(U,V)
      H=(((AL*COS(Q))+1.)**2.)+((AL*SIN(Q))*(AL*SIN(Q)))
```

```
      DE12=(2.*AL*SIN(Q))/(6.2831853*CO*CO*ZO*H*0.1E-08)
      DE13=(2.*AL*SIN(Q))/(6.2841853*CO*ZO*ZO*H)
      DE14=(2.*SIN(Q)*(1.-(AL*AL)))/(6.2831853*CO*ZO*H*H)
      DE15=((2.*AL*AL*AL*COS(Q))+(2.*AL*COS(Q))+(4.*AL*AL))
     4/(6.2831853*CO*ZO*H*H)
      F1=((DE12)*DCO)*((DE12)*DCO)
      F2=((DE13)*DZO)*((DE13)*DZO)
      F3=((DE14)*DL)*((DE14)*DL)
      F4=((DE15)*DQ)*((DE15)*DQ)
      FDE1=SQRT(F1+F2+F3+F4)
      DE22=(1.-(AL*AL))/(6.2831853*CO*CO*ZO*H*0.1E-08)
      DE23=(1.-(AL*AL))/(6.2831853*CO*ZO*ZO*H)
      DE24=((4.*AL)+((2.*COS(Q))*((AL*AL)+1.)))/(6.2831853*CO*ZO*H*H)
      DE25=((1.-(AL*AL))*2.*AL*SIN(Q))/(6.2831853*CO*ZO*H*H)
      Y1=((DE22)*DCO)*((DE22)*DCO)
      Y2=((DE23)*DZO)*((DE23)*DZO)
      Y3=((DE24)*DL)*((DE24)*DL)
      Y4=((DE25)*DQ)*((DE25)*DQ)
      FDE11=SQRT(Y1+Y2+Y3+Y4)
      WRITE(6,12)FE11,FE1,FDE1,FDE11
   12 FORMAT(14X,F11.4,14X,F11.4,14X,F11.4,18X,F11.4)
      IF(FE1-TE1)102,105,105
  103 IF(FE11-EFE11)5,4,4
    5 FE11=FE11+DFE11
      GO TO 3
    4 STOP
      END
```

```
$JOB  WATFIV   MAGDY
C     OPTIMUM VALUE OF CAPACITANCE
  108 PRINT109
  109 FORMAT(20X,'OPTIMUM VALUE OF CAPACITANCE')
      READ20,F1,F2,E1,E11
   20 FORMAT(4E14.8)
      READ21,ZO,COSS,COF,QCO
   21 FORMAT(4E14.8)
      READ22,DL,DQ,DZC,DCO
   22 FORMAT(4E14.8)
      READ23,QE1,QE11
   23 FORMAT(2F10.5)
  100 F=F1
  101 CO=COSS
  102 A=(CO*ZO*6.2831853*F*E11)
      B=(CO*ZO*6.2831853*F*E1)
      C=((1.+A)*(1.+A))+(B*B)
      AL=(SQRT((((1.-(A*A))-(B*B))*((1.-(A*A))-(B*B)))+(4.*B*B)))/C
      U=(2.*B)
      V=((1.-(A*A))-(B*B))
      Q=ATAN2(U,V)
      H=(((AL*COS(Q))+1.)**2.)+((AL*SIN(Q))*(AL*SIN(Q)))
      DK12=(2.*AL*SIN(Q))/(6.2831853*F*CO*ZO*CO*H)
      DK13=(2.*AL*SIN(Q))/(6.2831853*F*CO*ZO*ZO*H)
      DK14=(2.*SIN(Q)*(1.-(AL*AL)))/(6.2831853*F*CO*ZO*H*H)
      DK15=((2.*AL*AL*AL*COS(Q))+(2.*AL*COS(Q))+(4.*AL*AL))/
     2(6.2831853*F*CO*ZO*H*H)
      FF1=((DK12)*DCO)*((DK12)*DCO)
      FF2=((DK13)*DZO)*((DK13)*DZO)
      FF3=((DK14)*DL)*((DK14)*DL)
      FF4=((DK15)*DQ)*((DK15)*DQ)
      DE1=SQRT(FF1+FF2+FF3+FF4)
      DK22=(1.-(AL*AL))/(6.2831853*F*CO*CO*ZO*H)
      DK23=(1.-(AL*AL))/(6.2831853*F*CO*ZO*ZO*H)
      DK24=((4.*AL)+((2.*COS(Q))*((AL*AL)+1.)))/
     3(6.2831853*F*CO*ZO*H*H)
      DK25=((1.-(AL*AL))*2.*AL*SIN(Q))/(6.2831853*F*CO*ZO*H*H)
      Y1=((DK22)*DCO)*((DK22)*DCO)
      Y2=((DK23)*DZO)*((DK23)*DZO)
      Y3=((DK24)*DL)*((DK24)*DL)
      Y4=((DK25)*DQ)*((DK25)*DQ)
      DE11=SQRT(Y1+Y2+Y3+Y4)
      X=(QE1/DE1)
      Y=(QE11/DE11)
      PRINT1,X,Y,CO,F
    1 FORMAT(10X,'X=',F10.5,5X,'Y=',F10.5,5X,'CO=',E20.6,'F=',E20.6)
      IF(CO-COF)103,103,104
  103 CO=CO+QCO
      GO TO 102
  104 IF(F-F2)105,106,106
  105 F=F2
      GO TO 101
  106 GO TO 108
      END
```

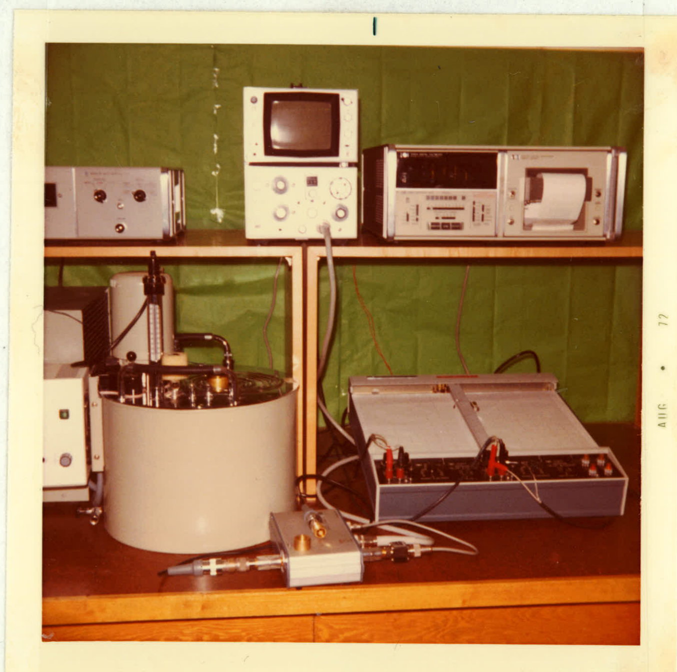

Plate 1. Experimental Setup.

Plate 2. The sample holder.